



# Physics-informed machine learning based RANS turbulence modeling convection heat transfer of supercritical pressure fluid

Yuli Cao, Ruina Xu, Peixue Jiang\*

*Key Laboratory for Thermal Science and Power Engineering of Ministry of Education, Key Laboratory for CO<sub>2</sub> Utilization and Reduction Technology of Beijing, Department of Energy and Power Engineering, Tsinghua University, Beijing 100084, China*



## ARTICLE INFO

### Article history:

Received 10 August 2022

Revised 21 October 2022

Accepted 31 October 2022

Available online 15 November 2022

### Keywords:

Machine learning

Turbulence modeling

Supercritical pressure

## ABSTRACT

Solving flow problems based on the Reynolds-averaged Navier-Stokes equations is a dominant method in terms of efficiency and accuracy for design and analysis of engineering applications, while the performance of RANS models in predicting the turbulent heat transfer of supercritical pressure fluid could be severely poor. To a great extent, the models are plagued by imperfect closures on higher order turbulence quantities with strongly varying thermal physical properties. This paper reports on an alternative approach to model the turbulent heat transfer at supercritical pressure, including the direct turbulent production models and the indirect transport closures using deep neural networks (DNN). This paper presents a method of modifying turbulence models of supercritical pressure fluid from high-fidelity simulation (DNS) data. An iterative DNS-DNN-RANS framework is proposed to establish explicit closures for turbulent momentum diffusion and turbulent thermal diffusion of turbulent heat transfer at supercritical pressure. Prior physics knowledge, feature engineering strategy and establish existing constitutive theory are involved to embed the special characteristics of supercritical pressure fluid into the turbulent closures to establish a proper regression system for machine learning (ML) algorithm. By embedding the explicit ML models, the low Reynolds number  $k-\varepsilon$  model was modified and was trained under a cross-case strategy with abundant DNS data. The modified model was successfully validated against DNS and experimental data for upward pipe flows, in which wall temperature were satisfactorily reproduced. The posterior simulations showed that the modified ML-KTVA model not only has a good performance in predicting the convection heat transfer of supercritical pressure fluid but also performs a favorable reproducibility of turbulence development in heat transfer deterioration cases.

© 2022 Published by Elsevier Ltd.

## 1. Introduction

With the rapid development of science and technology, the supercritical pressure fluid has been widely used in the field of industrial technology such as thermal power, utilization of nuclear energy, aerospace, and chemical engineering. The thermal-hydraulics of supercritical pressure fluid is an important topic in the development of the supercritical fluid application. Research on the supercritical pressure fluid flow and heat transfer in the vertical pipe has drawn extensive attention worldwide. Near the pseudo-critical point, the thermal physical properties of supercritical pressure fluid change dramatically with temperature and pressure, as shown in Fig. 1. In particular, the specific heat capacity exhibits a sharp peak at a temperature known as pseudo-critical

temperature,  $T_{pc}$ . The drastic variation of thermophysical properties and the induced buoyancy and flow acceleration effects will lead to nonlinear effects on the turbulent flow field and extremely complex convection heat transfer performance [1,2].

In these particular conditions, predicting the complex heat transfer behavior of supercritical pressure fluid, in which heat transfer deterioration and enhancement phenomena occur due to the complex effects, represents a considerable challenge for the present Computational Fluids Dynamics (CFD) code. Reynolds-averaged Navier-Stokes (RANS) simulations are still the dominant method of turbulence simulations. Low Reynolds number (LRN)  $k - \varepsilon$  turbulence models, such as the Launder and Sharma (LS) [4], Abe, Kondoh and Nagano (AKN) [5], and Myong and Kasagi (MK) [6] models are widely used in the simulation of turbulent heat transfer of supercritical pressure fluid. However, despite the LRN models depicting the local heat transfer deterioration and recovery qualitatively, studies showed that the common RANS turbulence models are unable to accurately calculate the heat transfer deterioration and recovery due to flow acceleration and buoyancy

*Abbreviation:* DNN, deep neural networks; DNS, direct numerical simulation; RANS, Reynolds-averaged Navier-Stokes; ML, machine learning.

\* Corresponding author.

E-mail address: [jiangpx@tsinghua.edu.cn](mailto:jiangpx@tsinghua.edu.cn) (P. Jiang).

## Nomenclature

$Bo^*$	buoyancy parameter, [= $Gr^*/(Re^{3.425}Pr^{0.8})$ ]
$c_p$	specific capacity at constant pressure
$C_{\varepsilon 1}, C_{\varepsilon 2}$	constants in the $\varepsilon$ -equation
$C_\mu$	constant in constitutive equation of eddy viscosity model
$D$	additional term in the $k$ -equation or diameter of pipe
$E$	additional term in the $\varepsilon$ -equation
$f_1, f_2$	functions in dissipation equation
$f_\mu$	damping function in the constitutive equation
$g$	acceleration due to gravity
$G_k$	buoyancy production
$Gr^*$	Grashof number, [= $\beta g D^4 q_w / (\lambda v^2)$ ]
$h$	heat transfer coefficient, [= $q_w / (T_w - T_b)$ ]; enthalpy
$k$	turbulent kinetic energy
$Kv$	flow acceleration parameter, [= $\frac{4q_w d \alpha_p}{Re^2 \mu_b c_p}$ ]
$p$	pressure
$P_k$	turbulent shear production
$Pr$	Prandtl number, [= $\mu c_p / \lambda$ ]
$q_w$	convective heat flux from the wall
$r$	radial coordinate
$R$	radius of pipe
$Re$	Reynolds number, [= $\rho u D / \mu$ ]
$T$	temperature
$u_x, u_r$	velocity components in $x, r$ -directions
$x$	axial coordinate
$y^*$	non-dimensional distance from pipe wall
<i>Greek symbols</i>	
$\varepsilon$	dissipation rate of $k$
$\kappa_t$	eddy diffusivity
$\lambda$	thermal conductivity
$\mu$	molecular viscosity
$\mu_t$	eddy viscosity
$\nu$	kinematic viscosity, [= $\mu / \rho$ ]
$\tau_w$	wall shear stress
$\rho$	density
$Pr_t$	turbulent Prandtl number
<i>Subscripts/over-bars</i>	
$0$	inlet
$b$	bulk
$f$	forced
$pc$	pseudo-critical
$t$	turbulence
$w$	wall
$'$	fluctuation
$\bar{\cdot}$	over-bar used for Reynold average
$\tilde{\cdot}$	over-bar used for Faver average

effects on the quantitative, leading to many difficulties for engineering design and analysis applications considering supercritical pressure turbulent heat transfer. The performance of RANS models in terms of predicting turbulent heat transfer of supercritical fluids were evaluated in some early studies: He et al. [7] conducted an assessment study on several LRN turbulence models in predicting the heat transfer and turbulence at supercritical pressure, and showed that predictions of the shear production of turbulence with different models varied considerably and that none of the models could produce reliable results for the buoyancy production of turbulence. Wen and Gu [8] performed a numerical investigation of heat transfer deterioration (HTD) in supercritical water by using six low-Reynolds number turbulence models, and showed that all

low-Reynolds models considered can to some extent reproduce the effect of buoyancy on heat transfer. But all  $k - \varepsilon$  type two-equation models seriously over-predict the heat transfer deterioration and do not reproduce the subsequent heat transfer recovery. Pucciarelli et al. [9] tested the performance of several two-equation turbulence models in solving the heat transfer of supercritical fluids, and showed that all of them are sensitive to the crossing of the critical temperature, but the recovery is not well predicted. Most of these turbulence models use the Boussinesq approximation and introduce one or two additional transport equations, for instance the Spalart-Allmaras model [10], the two-equation  $k - \omega$  model [11], and the SST model [12]. The models, to a great extent, are plagued by imperfect closures on higher order turbulence quantities with strongly varying thermal physical properties. The parameters and closure terms in the model are decided based on physics intuition from simple and subcritical pressure flow cases and often are focused on particular classes of problems, thus diminishing the predictive capabilities of a model in supercritical pressure conditions. The inaccuracy of the models could be attributed to two main reasons: (i) incorrect turbulence heat flux model in these turbulence models, i.e. the implementation of SGDH method and the usage of a constant  $Pr_t$ ; (ii) inaccurate prediction of turbulence production including shear production and buoyancy production. There exists a significant demand for improved RANS turbulence models in simulating supercritical pressure turbulent heat transfer.

Many efforts have been done to increase the prediction accuracy of turbulence models on the turbulent convective heat transfer at supercritical pressure, especially focused on heat transfer deterioration in upward flow. The major prospect and advancement of the modification of the turbulence model have been focused on the turbulent heat flux and the buoyancy production of turbulent kinetic energy. To improve the turbulent heat flux model, some new formulations of the turbulent Prandtl number ( $Pr_t$ ) in the energy equation had been proposed by Bae [13], Tang et al. [14], Tian et al. [15], Du et al. [16] and Mohsen and Bazargan [17]. The simulations showed better agreement in predicting heat transfer deterioration and enhancement to supercritical pressure fluid in these studies and proved that the modification of  $Pr_t$  in the buffer layer is the key to predicting the wall temperature accurately, since the modified  $Pr_t$  accommodates the contribution rate of molecular conduction to turbulent mixing on heat transfer. Moreover, using advanced hypotheses to evaluate the turbulent heat flux is an important topic. Kenjeres et al. [18], Xiong and Cheng [19] and Pucciarelli et al. [20] considered the anisotropic turbulent heat flux and conducted the simulation of heat transfer to supercritical fluids by the use of Algebraic Heat Flux Models (AHFM). Jiang et al. [21] implemented a new modified AKN model using a buoyancy effect model with an AHFM model for obtaining a better evaluation of the buoyancy turbulence production and a turbulent Prandtl number model for the SGDH model in the energy equation, the results showed improved performance in solving supercritical fluid heat transfer under buoyancy effects. A recent work performed by Pucciarelli et al. [20] showed that adopting the AHFM model even in the energy equation may lead to better results.

As for the turbulence production modeling, Koshizuka et al. [22] and He et al. [23,24] conducted numerical simulations of mixed convection to water and carbon dioxide at supercritical pressure in vertical tubes using numbers of low Reynolds number turbulence models, and found the production of turbulence kinetic energy due to buoyancy effects is significant to the heat transfer recovery. Zhao et al. [25], Mohseni and Bazargan [26] simulated heat transfer to supercritical pressure fluids for normal and buoyancy affected conditions using several low Reynolds number  $k - \varepsilon$  models and studied the influence of various aspects including the turbulent Prandtl number, the buoyancy production of turbulent

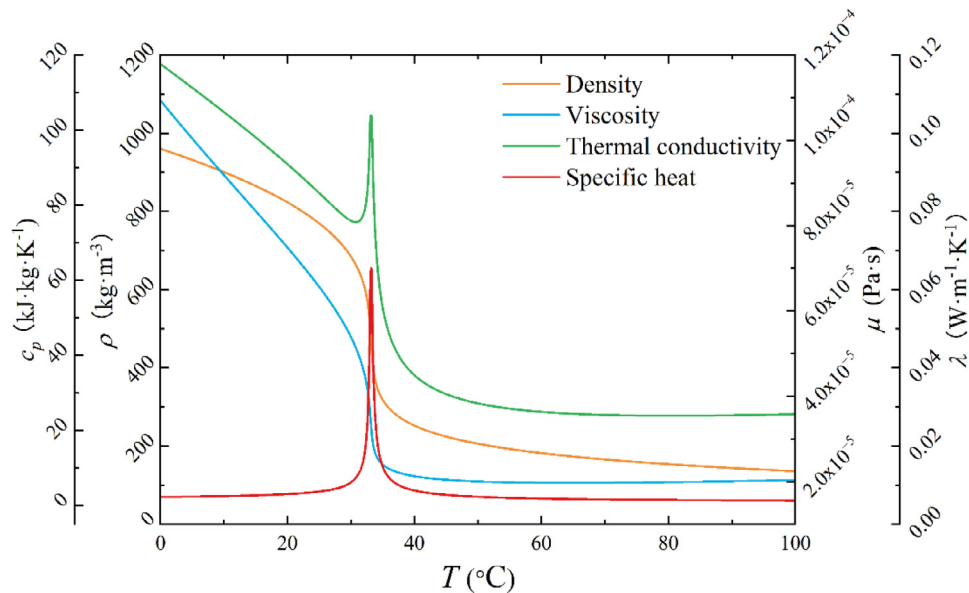


Fig. 1. Thermophysical properties of  $\text{CO}_2$  at 7.75 MPa [3].

kinetic energy, and the damping function in eddy viscosity model. Their study showed that the damping function had the greatest effect and is a priority for model modification, and provided guidelines for model development to more precisely predict buoyancy affected heat transfer. According to that, Mohseni and Bazargan [27] also modified the LRN turbulence model with the damping function, empirical coefficients, the turbulent Prandtl number and other terms. Considerable improvements have been achieved but it was hard to tell the rationality of modification of every single variable.

Moreover, 4-equation turbulence models have also been implemented, including two additional equations for the thermal fields to gain more accurate turbulent heat flux [9]. However, despite the greater sophistication, the potential benefits are limited. One reason is that the modification of the major parameters is based on physical intuition or analyzed from a small set of often idealized test cases. Even despite the additional degrees of freedom introduced in advanced turbulence models, the models are still “rigid” [28]—once the problem deviates from the set of calibration cases, the accuracy of the model will diminish. Therefore, a new and more effective paradigm is needed to insert the fundamental physics principle of turbulent heat transfer to supercritical pressure fluid into the RANS turbulence model.

To make an advanced modification of turbulence models, it is necessary to deeply understand the mechanism and collect the high-fidelity data of turbulence flow and heat transfer of supercritical pressure fluid. However, it's difficult to gain detailed information on the turbulence flow and thermal fields simultaneously at supercritical pressure through experimental techniques. Despite the inconvenience of experimental measurements, Direct numerical simulation (DNS) and Large Eddy simulation (LES) provided a promising and efficient method to obtain detailed information on turbulence flow and heat transfer in the cases considered. Bae et al. [29–31] carried out a number of DNS studies of heated vertical pipe flows of SCP  $\text{CO}_2$ . It was shown that under the buoyancy effects the normalized streamwise velocity profiles changed and the turbulent shear stress near the wall is largely reduced. A detailed picture of SCP turbulence structures was obtained and showed that the high-speed and low-speed fluctuating velocity streaks disappear at the locations of the HTD, meanwhile the turbulence activities such as sweep and ejection decreased. The external (indirect) and structural (direct) effects of buoyancy on turbulence and turbulent heat flux had been studied. According to Petukhov et al. [32], the external effect of buoyancy acts as a body force in the mean velocity equation, and the structural effect of buoyancy acts as the buoyancy production in the budget of turbulence kinetic energy. The former results in a promotion or destruction of turbulence production, which was known to be the dominating effect of flow laminarisation and recovery. However, recent DNS data proved that the structural effect of buoyancy is either a considerable factor for turbulence recovery, which provided a significant guideline for turbulence modeling to improve the prediction accuracy. Nemati et al. [33,34] used DNS to study the effect of large variations in thermophysical properties on developing turbulent pipe flows with supercritical pressure fluid, and concluded that large property variations will cause an increase of wall-normal velocity fluctuations and thus an increased overall heat flux and skin friction. The turbulence activity discussed in both high and low buoyancy cases is consistent with Bae et al. [29–31]. Peeters et al. [35,36] conducted DNS of supercritical pressure thermal flow in an annular channel with a heated outer wall and a cooled inner wall, and analyzed the budget of the turbulent heat transfer and the mechanism of near-wall turbulence regeneration. First, the authors demonstrated that not only the mean stratification but also the large instantaneous thermophysical property variations have an important influence on the self-regeneration process of near-wall turbulence. Then, they concluded that both the fluctuations and the mean gradients of the density and molecular Prandtl number had a significant influence on the turbulent heat flux, therefore the direct effect could be either important.

More recently, DNS studies conducted by He et al. [37] investigated the unified explanation for the various flow laminarization mechanisms in a heated pipe flow, using non-uniform body forces theory [38], and stated that the buoyancy generation is dominating in the re-transition region. Cao et al. [39] carried out direct numerical simulations on turbulent heat transfer under the coupling effects of buoyancy and thermal accelerations, considering both upward flow and downward flow. They pointed out that the double peaks of turbulence production are necessary for the turbulence regeneration in the region of heat transfer recovery. Besides, the LES study by Niceno and Sharabi [40] on turbulent heat transfer at supercritical pressures also conducted a detailed investigation

on the mechanism of turbulence deterioration/recovery that can be used to support the RANS turbulence modeling.

Compared to RANS simulations, high-fidelity simulations such as DNS and LES are less convenient and popular in engineering applications due to their high computational costs. But the latest physics knowledge and dataset obtained through the high-fidelity simulations offered a solid fundamental for the advanced turbulence model development leverage. With increasing amounts of high-fidelity simulation data from DNS and LES, detailed information of both averaged and turbulent flow fields can be obtained close to real physical conditions, providing a high-precision database as well as the mechanism for RANS turbulence modeling [67]. Concurrently, the rise of the machine learning (ML) method provides inspiration for processing and synthesizing large quantities of data, promoting the promising approach of RANS turbulence modeling based on the data-driven method. In general, turbulence modeling mainly focused on turning a set of deterministic closure coefficients using Bayesian averaging and uncertainty quantification, and making hypotheses based on physical intuition. Unlike the traditional way, ML-based turbulence modeling can improve the performance of RANS simulations by utilizing data generated from large quantities of computational and physical experiments that encompass the generalized physical information of various conditions and geometries, capturing the underlying correlation behind data and avoiding the limitations of the traditional forms of turbulence closures.

Recent studies have demonstrated the ability of ML algorithms to reconstruct RANS turbulence closures utilizing high-fidelity simulation data [28,41,42]. Contemporary work employing ML methodologies in RANS turbulence modeling can be grouped into two distinct uses, to extract governing equations from data and to construct surrogates of closure relations. Brunton, Proctor and Kutz [43] developed a sparse regression to recover Navier-Stokes equations underlying a nonlinear dynamical system with time-series data. The authors demonstrated that the data-driven discovery of dynamics will continue to play an important role in turbulence solving. Duraisamy et al. [44–46] utilized neural network to construct a functional form of correction coefficients in the turbulence transport equation in the Spalart-Allmaras(S-A) model and transitional  $k-\omega$  model, in which successful reproductions of the training cases were achieved. As for the constitutive relations modeling, present works followed the general effective-viscosity hypothesis and relied on supervised learning with the training data from DNS or LES. Weatheritt et al. [47–49] proposed a framework using a gene expression program to search for an optimal algebraic expression formula for the tensorial combination coefficients. Their model utilized data from a large-eddy simulation of a low-pressure turbine wake flow and showed encouraging results against isotropic models. Liu et al. [50] used non-parametric ML models (i.e., neural network) to build a regression model for eddy-viscosity. The posterior simulations of channel flow and flow over periodic hills demonstrate improved performance compared with the  $k-\omega$  SST model, even though the test condition is beyond the trained data. While in the application of ML models with the constitutive relations in the turbulence transport equations, the effective form of the RANS closure term and the multi-valued problem of the general constitutive hypothesis should be paid special attention to Ling et al. [51,52]. To ensure consistency between a model's a priori and a posteriori performance, the physics-informed ML framework of Wang, Wu and Xiao [53] and Wu et al. [54] derived an eddy-viscosity-based decomposition form of the closure term.

To sum up, traditional RANS turbulence models, using pre-specified functional forms evolved from the knowledge of the limited flow physics and the intuition of the turbulence model developers, have limitations in simulations of supercritical pressure turbulent heat transfer. Nowadays, developing ML techniques and

a tremendous number of high-fidelity databases from high precision numerical methods provide a novel and encouraging perspective for RANS turbulence modeling. The existing studies about ML-driven RANS modeling mainly focus on pure flow with constant properties. While the turbulence convection heat transfer of supercritical pressure fluid involves the complex interaction of turbulent dynamics and heat transfer process, the turbulence model based on constant physical fluid flow has poor prediction performance in this kind of problem. This work is aimed at creatively transplanting the underlying mechanism of turbulent convection heat transfer of supercritical pressure fluid from the original DNS data to the RANS model using the machine learning method.

In the present study, the primary target is to propose a novel physics-informed machine learning based turbulence modeling approach with low computational cost and high accuracy. The ML algorithm is constructed to create explicit closures for turbulence equation of heated supercritical pressure flow by utilizing data generated from a suite of DNS data encompassing a wide variety of flow conditions including normal heat transfer, heat transfer deterioration as well as heat transfer enhancement. Moreover, the viable approach of combining ML algorithm with CFD numerical simulation is addressed. By embedding the deep neural network (DNN) model into the existing low Reynolds number  $k-\varepsilon$  model in CFD solvers, we established an iterative DNS-DNN-RANS framework to enable the representable ML models of turbulence to improve the predictive capabilities. The detailed posterior simulations have been done to demonstrate that the modified model not only has a good performance in predicting the convection heat transfer of supercritical pressure fluid but also performs a favorable reproducibility of turbulence development in heat transfer deterioration cases.

## 2. Methodology

### 2.1. DNS-DNN-RANS framework

In this section, we introduce a general introduction to the iterative DNS-DNN-RANS framework for RANS turbulence modeling with ML algorithm. The research has been pursued in formulating and applying the proposed framework to develop closure models to close conservation equations in RANS simulations. Machine learning refers to a class of methods for creating models from data. In our works, the high-fidelity data utilized for ML is from abundant DNS studies (Cao et al. [39], Yan et al. [55], Bae et al. [29]), which have been adequately evaluated and trustworthy. The ML algorithm used to apply the data-driven method to DNS data is DNN. The iterative DNS-DNN-RANS framework consists of three processes including data processing, training and prediction phase (see Fig. 2). First, the simulation data considering a wide variety of heat transfer conditions and effects need to be collected, categorized, and normalized, to build an integrated and abundant training database that encompasses the underlying knowledge of heat transfer mechanisms at supercritical pressure. Second, the importance of each flow quantity included in turbulent heat transfer needs to be assessed, to establish the effective form of the input features for the RANS closure term. Third, the DNN algorithm will be applied to recognize the underlying correlations from the training data and generate the learned representable function of the target turbulence closures. After that, the so-developed "networks" will be embedded into RANS solvers to enable turbulent heat transfer simulation of supercritical pressure fluid.

For the large amount of high-fidelity data acquired for the machine learning process, it has to undergo several data processing steps. Since DNS can provide the most detailed information on turbulence flow and temperature field, the obtained data could be tremendous. If the original simulation data is utilized as the train-

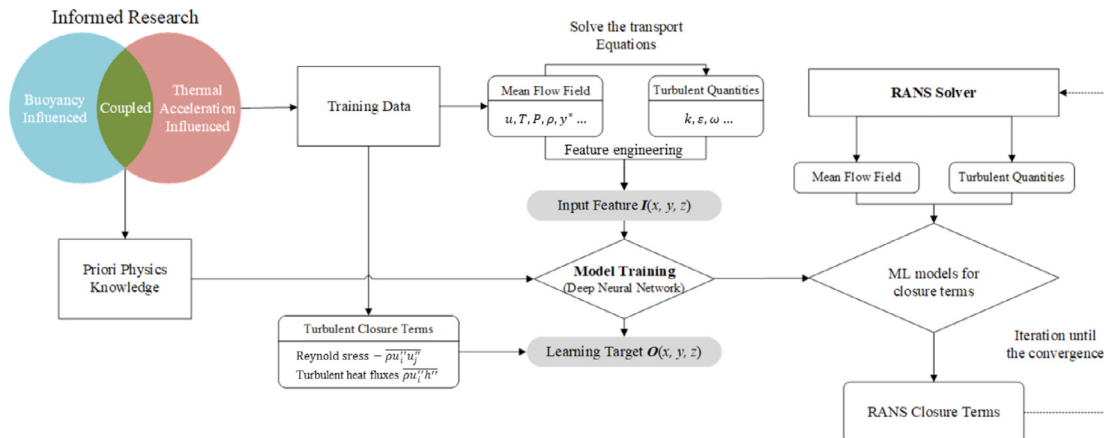


Fig. 2. The iterative DNS-DNN-RANS framework.

ing database directly, it might induce feature dimension explosion and poor performance of the machine learning model. Therefore, it's of great significance to implement feature engineering on the training data before the training phase to improve the performance of the ML-base model. Feature processing can be divided into the following three methods: feature design, feature extraction and feature selection. Feature construction refers to finding out the features with practical significance manually from the original data based on informed physics knowledge and sometimes physics intuition. Feature extraction is a process of automatically reducing the dimension of the original observation to make its feature set small enough to be modeled. Usually, principal component analysis (PCA) and linear discriminant analysis (LDA) can be used. Different features have different effects on the accuracy of the model. Some features are irrelevant to the problem to be solved, and some features are redundant information, which should be removed. Feature selection is the process of automatically selecting the subset of features that are most important to the problem. The commonly used feature selection methods can be divided into three categories: filter, wrapper and embedded. Based on informed physics knowledge, the key closure terms of the RANS turbulence model in describing the heated turbulent heat transfer of supercritical pressure fluid, which encompasses a variety of conditions with buoyancy and thermal acceleration effects, are constructed as the machine learning target. The features indicating the core characteristic in relation to the target turbulence closure are selected and normalized to compose the input feature  $I(x, y, z)$  of machine learning.

In general RANS simulation for incompressible heated flow, there are four Reynolds averaged Navier-Stokes equations together with one energy equation to be solved. While solving the Reynolds equations and energy equation in an iterative manner, the unclosed Reynolds stresses and turbulent heat fluxes used to be determined either via constitutive relations or directly from modeled transport equation. In the predicting phase in Fig. 2, the unclosed turbulence quantities are calculated with the well-established representable DNN models integrated into the RANS solver instead of the original relations. The procedure of the iterative loop is shown in Fig. 3, in which the subscript  $n$  represents the current iteration and  $n-1$  represents the previous iteration. For each iteration, the ML model receives the input field  $I(x, y, z)$  calculated at step V and returns the output field  $O(x, y, z)$  to update the closure terms in the turbulence model and then solve the turbulence transport equations using the updated closure terms and mean field  $(u_i^n, T^n, p^n)$ . For each iteration, all of the steps in the loop are run. The solver is iterated until the iterative loop is broken through the condition.

The detailed methodology used in the DNS-DNN-RANS framework will be discussed in the following section. The brief introduc-

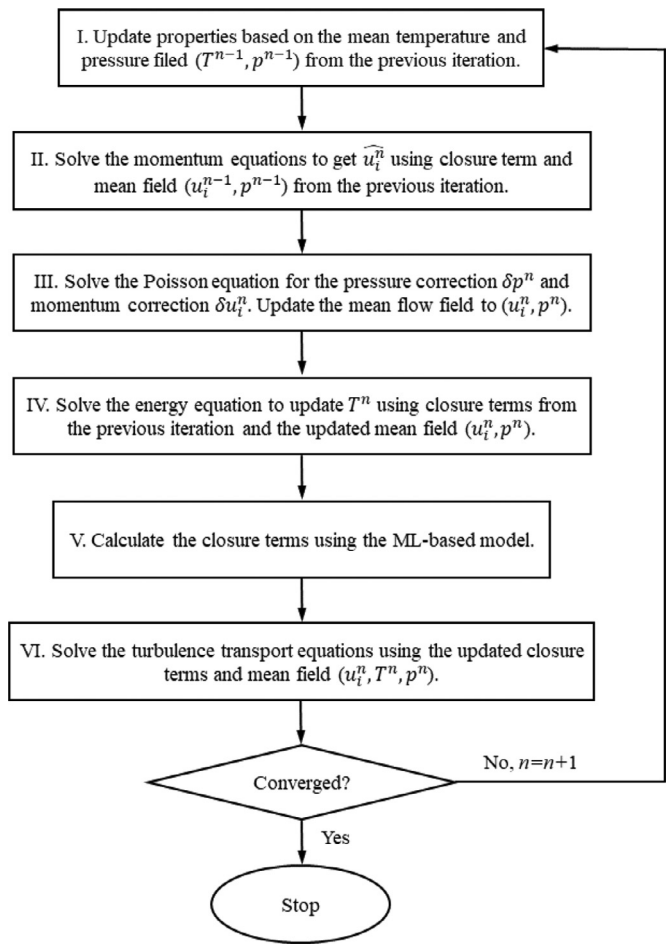


Fig. 3. The procedure for the iterative loop.

tion to the turbulence modeling of turbulent stress and turbulent heat flux is given in Section 2.2, and the ML methods of training the DNN model are introduced in Section 2.3.

## 2.2. Turbulence modeling

The present work is mainly aimed at the low-Reynolds number two-equation  $k-\varepsilon$ RANS model based on the general eddy viscosity hypothesis. The researchers first calculated the introduced correction coefficient or the added source term according to the

**Table 1**  
Definition in the AKN model (Baseline model).

$C_\mu$	$C_{\varepsilon 1}$	$C_{\varepsilon 2}$	$\alpha_k$	$\alpha_\varepsilon$	$D$	$E$	Wall B.C.
0.09	1.5	1.9		1.4	1.4	0	$k_w = 0, \varepsilon_w = 2\nu \frac{k}{y^2}$
$f_\mu$				$f_1$		$f_2$	
$[1 + \frac{5}{Re_t^{0.75}} \exp(-(\frac{Re_t}{200})^2)](1 - \exp(-\frac{y}{14}))^2$		1.0			$\{1 - 0.3 \exp(-(\frac{Re_t}{65})^2)\}[1 - \exp(-\frac{y}{3.1})]^2$		

Note:  $Re_t = \frac{k^2}{\nu \varepsilon}, y^* = \frac{y}{\nu} (\nu \varepsilon)^{0.25}, \tau_w = \mu \frac{du}{dy}$ .

high-resolution data, and then used this as the learning target to build a data-driven model and coupled it with the solver. We are particularly concerned with low-Reynolds number eddy viscosity turbulence models since according to earlier studies it's necessary to simulate the near-wall non-equilibrium flows for supercritical pressure turbulent heat transfer. The low Reynolds number eddy viscosity turbulence model, the Abe, Kondoh and Nagano (AKN) [5] model which includes the modeling of the effects of the wall region as well as the core, were selected for use in the present study. The steady-state governing equations for continuity, momentum and energy are as follows:

$$\frac{\partial}{\partial x_i} (\rho \bar{u}_i) = 0 \quad (1)$$

$$\frac{\partial}{\partial x_j} (\rho \bar{u}_i \bar{u}_j) = -\frac{\partial \bar{T}}{\partial x_i} + \rho g_i + \frac{\partial}{\partial x_j} \left[ \mu \left( \frac{\partial \bar{u}_i}{\partial x_j} + \frac{\partial \bar{u}_j}{\partial x_i} \right) - \rho \bar{u}'_i \bar{u}'_j \right] \quad (2)$$

$$\frac{\partial}{\partial x_i} (\rho \bar{u}_i c_p \bar{T}) = \frac{\partial}{\partial x_i} (\lambda \frac{\partial \bar{T}}{\partial x_i} - \rho c_p \bar{u}'_i \bar{T}') \quad (3)$$

where  $-\rho \bar{u}'_i \bar{u}'_j$  refers to the turbulent stress tensor and  $-\rho \bar{u}'_i \bar{T}'$  refers to the turbulent heat flux vector. Here,  $u'_i$  and  $T'$  are respectively the turbulent fluctuations of velocity and temperature. These two terms appear as unknowns in the governing equations and are determined in the  $k - \varepsilon$  model via the eddy viscosity hypothesis. According to the Boussinesq hypothesis, the Reynolds stresses are given by:

$$-\rho \bar{u}'_i \bar{u}'_j = \mu_t \left( \frac{\partial \bar{u}_i}{\partial x_j} + \frac{\partial \bar{u}_j}{\partial x_i} \right) - \frac{2}{3} k \delta_{ij} \quad (4)$$

in which the eddy viscosity  $\mu_t$  is:

$$\mu_t = \rho \nu_t = \rho C_\mu f_\mu \frac{k^2}{\varepsilon} \quad (5)$$

As it is supposed that the eddy viscosity depends on the turbulence quantities  $k$  and  $\varepsilon$ , thus the model transport equations of  $k$  and  $\varepsilon$  are solved. The general form of the equations can be expressed as follow. Note that the definitions of the correction functions,  $D$  and  $E$ , the boundary conditions, the model constants and the damping functions,  $f_\mu$ ,  $f_1$  and  $f_2$  in the present AKN model are given in Table 1.

$$\frac{\partial}{\partial x_i} (\rho \bar{u}_i k) = \frac{\partial}{\partial x_i} \left[ (\mu + \frac{\mu_t}{\sigma_k}) \frac{\partial k}{\partial x_i} \right] + P_k + G_k - \rho \varepsilon + \rho D \quad (6)$$

$$\frac{\partial}{\partial x_i} (\rho \bar{u}_i \varepsilon) = \frac{\partial}{\partial x_i} \left[ (\mu + \frac{\mu_t}{\sigma_\varepsilon}) \frac{\partial \varepsilon}{\partial x_i} \right] + C_{\varepsilon 1} f_1 \frac{\varepsilon}{k} (P_k + G_k) - C_{\varepsilon 2} f_2 \frac{\rho \varepsilon^2}{k} + \rho E \quad (7)$$

in which  $P_k$  and  $G_k$  are the turbulent kinetic energy produced by shear stress and buoyancy, respectively. The expressions follow:

$$P_k = -\rho \bar{u}'_i \bar{u}'_j \frac{\partial \bar{u}_i}{\partial x_j} \quad (8)$$

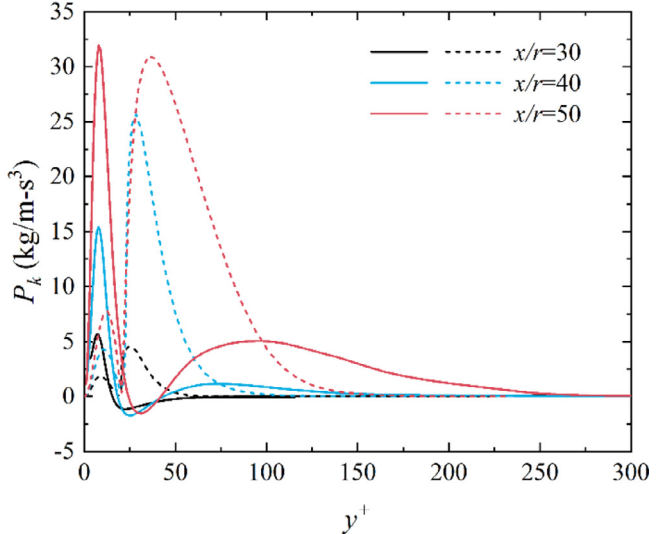


**Fig. 4.** Comparison of turbulence production,  $P_k$ . (Solid line: DNS [29]; Dashed line: AKN)

$$G_k = g_i \bar{\rho}' \bar{u}'_i = -\rho \beta g_i \bar{u}'_i \bar{T}' \quad (9)$$

For turbulent heat flux  $\rho \bar{u}'_i \bar{T}'$  in Eqs. (3) and (9), it is generally calculated based on the simple gradient diffusion hypothesis (SGDH) model in the YS and AKN models used in the present study. This model represents the scalar flux vector with a Fourier-like equation

$$\bar{u}'_i \bar{T}' = -\kappa_t \frac{\partial \bar{T}}{\partial x_i} = -\frac{\nu_t}{Pr_t} \frac{\partial \bar{T}}{\partial x_i} \quad (10)$$

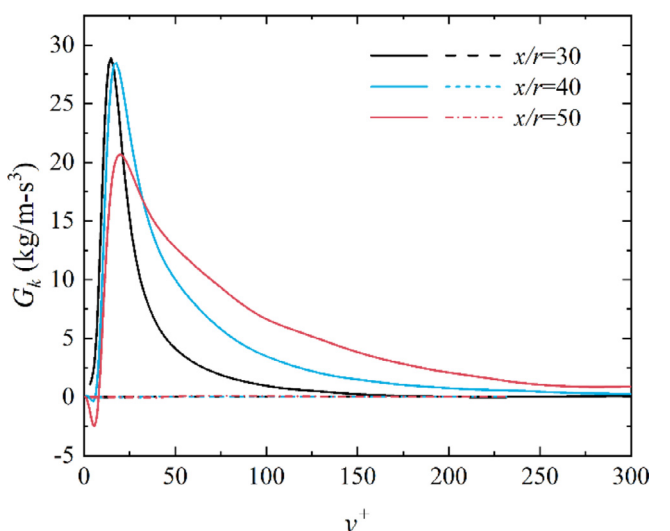
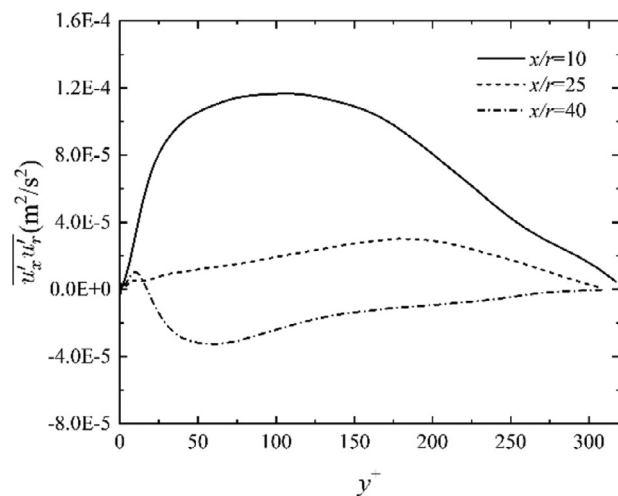


**Fig. 5.** Comparison of buoyancy production,  $G_k$ . (Solid line: DNS [29]; Dashed line: AKN).

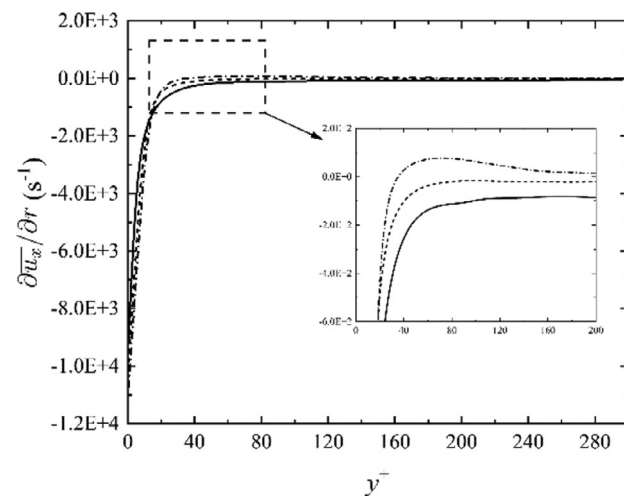
Where  $\kappa_t$  is the eddy diffusivity,  $\text{Pr}_t$  is the turbulent Prandtl number defined as the ratio of the turbulent eddy viscosity to the eddy diffusivity. In practice, a constant value is widely used to prescribe it, for non-metallic fluids ( $\text{Pr}_t \sim 0.7$ ) in the boundary layer and pipe flow. This is done for the reasons of simplicity, the lack of better information, and in view of the fact that the approach has been found to yield satisfactory results. The usual assumption is 0.85 in the AKN model.

In the turbulent heat transfer at supercritical pressure, buoyancy force and flow acceleration will lead to changes in flow field structure, and the development of turbulence and turbulent volume transport is significantly affected. Due to the complexity of the physics involved, the model of both turbulent stress and turbulent heat flux described above is not appropriate. As shown in Figs. 4 and 5, the turbulence production  $P_k$  and buoyancy production  $G_k$  in Case C of Bae et al. [29] show a great difference between the DNS results and simulation results using the AKN turbulence

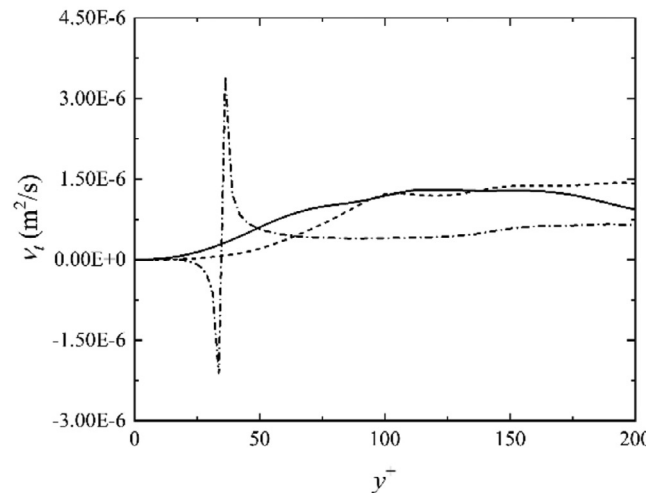
model based on the eddy viscosity and simple gradient diffusion hypothesis. The DNS results of  $P_k$  show big attenuation at  $x/r=30$  and regeneration with two peaks at  $x/r=40$  and 50. The AKN result of  $P_k$  is smaller than DNS at the first peak and shows two production peaks already at  $x/r=30$ . According to an earlier study, the first peak near the wall plays a dominant role in producing turbulence. While the turbulence starts to recover due to the M-shaped velocity profile the turbulence production  $P_k$  increases with a second peak far from the wall. The first peak of  $P_k$  is underdeveloped, while the second peak is too large from the AKN model, which can be attributed to the inaccurate model of turbulent stress  $-\rho u' i u' j$ . For the buoyancy production  $G_k$  in Fig. 5, the AKN results of  $G_k$  are almost zero compared to the DNS results, failing to promote the turbulence production as the direct effect of buoyancy force. That's because the axial gradient of temperature is small in the heated vertical tube, the SGDH model using the constant Prandtl number is hard to calculate the correct turbulent heat flux  $\rho u' i T'$ .



(a)



(b)



(c)

**Fig. 6.** Turbulent stress quantities for Case C from DNS [29]. (a) Turbulent stress  $\overline{u'_x u'_r}$ , (b) Radial gradient of axial velocity  $\frac{\partial \overline{u_x}}{\partial r}$ , (c) The eddy viscosity  $\nu_t = -\overline{u'_x u'_r} / (\frac{\partial \overline{u_x}}{\partial r} + \frac{\partial \overline{u_r}}{\partial x})$ .

therefore the buoyancy production  $G_k$ . More complicated models of turbulent heat flux have been proposed such as the generalized gradient diffusion hypothesis (GGDH) model by Ince and Launder [57] and the algebraic heat flux model (AHFM) by Zhang et al. [58]. However, viable solutions for heat and mass transfer simulation of complex flows are limited using these traditional form models.

Further investigation has been conducted, the distribution of the turbulent stress and the turbulent heat flux of DNS results has been given in Figs. 6 and 7 at three positions  $x/r=10$ ,  $x/r=25$  and  $x/r=40$ , which refers to buoyancy influenced negligible period, buoyancy influenced deteriorated period, buoyancy influenced regenerated period respectively. Note that in the case of heated tube flow, the Reynolds shear stress,  $-\rho\bar{u}'_x\bar{u}'_r$ , has a dominant contribution to the RANS equation, which is mainly determined by eddy viscosity  $\nu_t$  and mean strain rate tensor  $S_{ij}$ . There are three conclusions should be incorporated into the turbulence modeling:

- (1) For flow periods before the M-shaped velocity profiles appear, the diffusion of the turbulent stress  $-\rho\bar{u}'_x\bar{u}'_r$  and the radial turbulent heat flux  $\rho\bar{u}'_rT'$  follow the Reynolds analogy. But the ratio  $Pr_t$  of the eddy viscosity and the eddy diffusivity is not constant.
- (2) The turbulent heat flux presents anisotropy and is not always aligned with the gradients of the mean temperature. The magnitude of axial turbulent heat flux  $\rho\bar{u}'_xT'$  is much larger than the radial turbulent heat flux  $\rho\bar{u}'_iT'$ , particularly in the near-wall region. At position  $x/r=25$ ,  $\frac{\partial T}{\partial x}$  is positive but  $\rho\bar{u}'_xT'$  changes to reverse resulting in the positive buoyancy production. Consequently, the eddy diffusivity model would give serious error in buoyancy-influenced flows.
- (3) After the M-shaped velocity profiles appear, there are zero points in the distributions  $\frac{\partial \bar{u}_x}{\partial r}$ , while  $\frac{\partial \bar{u}_r}{\partial x}$  is negligible. The eddy viscosity is defined as  $\nu_t = -\bar{u}'_x\bar{u}'_r / (\frac{\partial \bar{u}_x}{\partial r} + \frac{\partial \bar{u}_r}{\partial x})$  encountering numerical discontinuity at the position where the gradient across 0. Note that the Reynolds analogy is not applicable under this situation.

In the original LRN  $k-\varepsilon$  model, as shown in Fig. 8, the eddy viscosity  $\nu_t$  is always positive so as  $P_k$ . What's more, it increases incorrectly in the buffer layer since the eddy viscosity model doesn't consider the influence of the velocity profile curvature. This can explain why the second peak of the turbulence production  $P_k$  is overestimated.

Having said all of above, either the eddy viscosity model or the SGDH model is inappropriate for simulation of the turbulent stress and the turbulent heat flux, respectively, for the heated turbulence at supercritical pressure especially with complex effects of buoyancy and thermal acceleration. Therefore, it is of critical importance to model the RANS closure term with a nonlinear eddy-viscosity approach, underlying the more complicated turbulent stress and scalar-flux transport under buoyancy and thermal acceleration.

### 2.3. Model formulation

The proposal we wish to advance through this paper is that an explicit algebraic relation for turbulent closures may be constructed. First, the model for eddy viscosity  $\nu_t^*$  and eddy diffusivity  $\kappa_t^*$  are constructed to replace the existing one in the original LRN model. Because the commercial software ANSYS FLUENT did not allow eddy viscosity and eddy diffusivity anisotropy to be implemented in the energy equation introducing corrective sources to simulate the presence of anisotropy may result numerically impossible. As a consequence, for momentum and energy equations the general eddy viscosity hypothesis and simple gradient diffusion hypothesis remain to simulate the turbulent Reynolds stress and

turbulent heat flux. Second, the model for turbulent production terms  $P_k$  and  $G_k$  are constructed to directly insert into the transport equation of turbulence kinetic energy and turbulence dissipation rate.

In this section, we aim at constructing proper ML regression systems for the learning targets: (1) scaled eddy diffusivity  $\kappa_t^*$ , (2) scaled eddy viscosity  $\nu_t^*$ , (3) scaled turbulence buoyancy production term  $G_k^*$ , (4) scaled turbulence shear production term  $P_k^*$ . Individual neural networks reproduce the distribution of each target, whose distribution over the computational domain is determined before training. The estimation of the dimensional outputs is computed from the high-fidelity database:

$$\begin{aligned}\kappa_t^h &= \left(\bar{u}'_r T'\right)^h / \left(\frac{\partial T}{\partial r}\right)^h, \nu_t^h = -\left(\bar{u}'_i \bar{u}'_j\right)^h / 2S_{ij}^h, \\ G_k^h &= -\left(g_i \bar{u}'_i \bar{u}'_i\right)^h, P_k^h = -\left(\rho \left(\bar{u}'_i \bar{u}'_j\right) \frac{\partial \bar{u}_i}{\partial x_j}\right)^h\end{aligned}\quad (11)$$

The superscript  $h$  denotes the high-fidelity quantities from DNS Reynolds averaged data. Taken as the learning target for the ML regression model, the features have been scaled to maintain the generalizability of the model:

$$\begin{aligned}P_k^* &= \frac{P_k^h}{\rho_0 U_0^3 / L_0}, G_k^* = \frac{G_k^h}{\rho_0 U_0}, \\ \nu_t^* &= \frac{\nu_t^h}{U_0 L_0}, \kappa_t^* = \frac{\kappa_t^h}{U_0 L_0}\end{aligned}\quad (12)$$

where the superscript \* refers to nondimensional quantities, the subscript 0 refers to the inlet condition with the inlet bulk velocity being denoted by  $U_0$ , and  $L_0$  is the tube radius.

Before constructing a proper machine learning system, the functional relationships between the learning targets and various tensor quantities are obtained from the transport equations and tensor representation theory. The rationally assumed functional relationship implied from the transport equation is then reduced with prior physics knowledge, and feature engineering strategy. The exact transport equations for turbulent Reynolds stress and turbulent heat flux are as follows:

#### Turbulent Reynolds stress

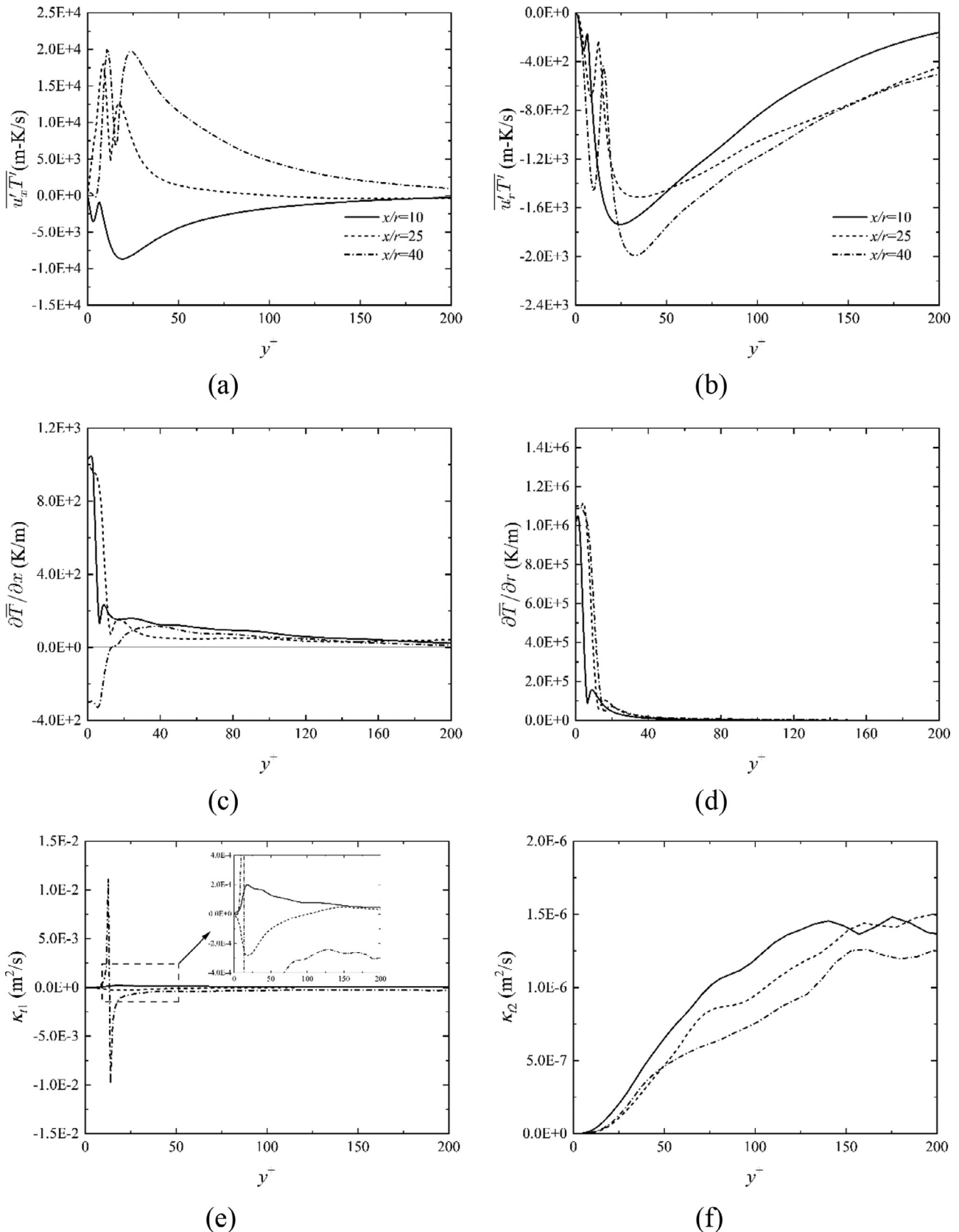
$$\begin{aligned}\frac{\partial(\rho \bar{u}_k \bar{u}'_i \bar{u}'_j)}{\partial x_k} &= -\overline{\rho u''_i u''_k} \frac{\partial \bar{u}_j}{\partial x_k} - \overline{\rho u''_j u''_k} \frac{\partial \bar{u}_i}{\partial x_k} + p' \left( \frac{\partial \bar{u}'_i}{\partial x_j} + \frac{\partial \bar{u}'_j}{\partial x_i} \right) \\ &- \frac{\partial}{\partial x_k} \left( \overline{p' u''_i} \delta_{jk} + \overline{p' u''_j} \delta_{ik} + \overline{\rho u''_i u''_j u''_k} - \mu \frac{\partial \bar{u}'_i \bar{u}'_j}{\partial x_k} \right) \\ &- 2\mu \left( \frac{\partial \bar{u}'_i}{\partial x_k} \frac{\partial \bar{u}'_j}{\partial x_k} \right) - \rho g_i \beta \bar{u}'_j T' - \rho g_j \beta \bar{u}'_i T'\end{aligned}\quad (13)$$

#### Turbulent heat flux

$$\begin{aligned}\frac{\partial(\rho \bar{u}_k \bar{u}'_i T')}{\partial x_k} &= -\overline{\rho T' u'_k} \frac{\partial \bar{u}_i}{\partial x_k} - \overline{\rho u'_i u'_k} \frac{\partial T'}{\partial x_k} - \rho \beta g_i \overline{T'^2} - \rho(a + v) \frac{\partial T'}{\partial x_k} \frac{\partial u'_i}{\partial x_k} \\ &- \frac{\partial}{\partial x_k} \left( \overline{p' T'} \delta_{jk} + \overline{\rho a u'_i} \frac{\partial T'}{\partial x_k} + \overline{\rho u'_i u'_k T'} - \mu \overline{T'} \frac{\partial u'_i}{\partial x_k} \right) - \overline{p' \frac{\partial T'}{\partial x_k}}\end{aligned}\quad (14)$$

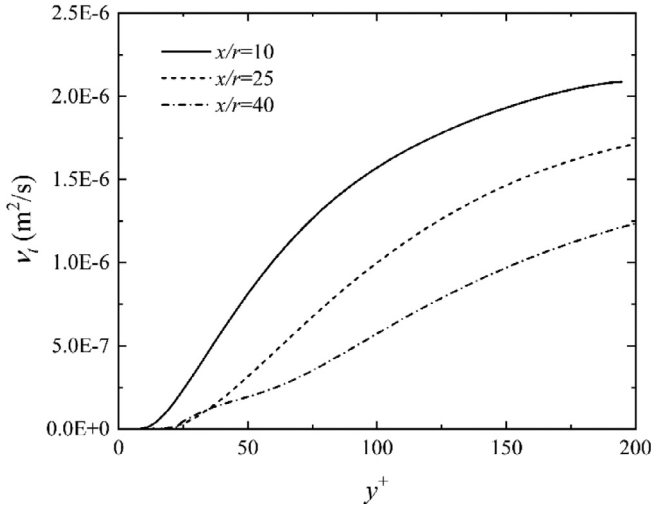
where  $u''$  indicates the fluctuating part of velocity with Farve averaging,  $v$  is the kinematic viscosity,  $\beta$  is the volumetric expansion coefficient,  $a$  is the thermal diffusivity,  $\rho$  is the fluid density and  $p'$  is the fluctuating pressure. Among the Reynolds stress and turbulent heat flux components,  $\rho u''_x u''_x$ ,  $\rho u''_x u''_r$  and  $\rho u'_x T'$  are directly affected by the gravitational force term in vertical flows.

The terms on the RHS consist of the production term, the viscous term, the turbulent-transport term and the pressure-gradient term. Proceeding from left to right, there are three distinct groupings of terms in Eqs. (13) and (14): one which is associated with purely turbulence interactions, the second which involves interactions between the mean velocity/temperature gradients and fluctuating quantities and a third which involves the body forces. For



**Fig. 7.** Turbulent heat flux quantities for Case C from DNS [29].

(a) Axial turbulent heat flux  $\overline{u'_x T'}$ , (b) Radial turbulent heat flux  $\overline{u'_r T'}$ , (c) Axial gradient of temperature  $\partial \bar{T} / \partial x$ , (d) Radial gradient of temperature  $\partial \bar{T} / \partial r$ , (e) The eddy diffusivity  $\kappa_{t1} = -\overline{u'_x T'} / \partial \bar{T} / \partial x$ , (f) The eddy diffusivity  $\kappa_{t2} = -\overline{u'_r T'} / \partial \bar{T} / \partial r$ .

Fig. 8. The eddy viscosity  $v_t$  for Case C [29] using the AKN model.

the general case of supercritical pressure heated flow where the effects of the gravitational field are important, we can generalize the general set of influencing features, the functional relationship is implied by Eqs. (13) and (14):

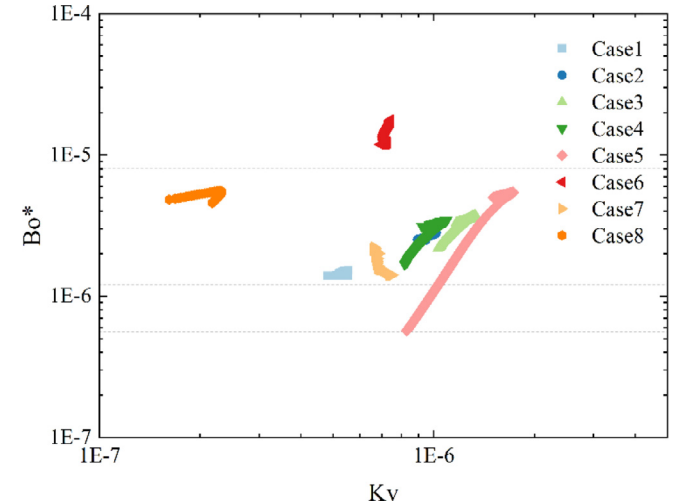
$$-\bar{u}''_i \bar{u}''_j = f_1(\bar{u}_i, S_{ij}, W_{ij}, \rho, \mu, \bar{T}, h, k, \varepsilon, g_i, \frac{\partial \bar{T}}{\partial x_j}, \frac{\partial \rho}{\partial x_j}, y^*) \quad (15)$$

$$-\bar{u}'_j \bar{T}' = f_2(\bar{u}_i, S_{ij}, W_{ij}, \rho, \mu, \bar{T}, \bar{u}''_i \bar{u}''_j, h, k, \varepsilon, g_i, \frac{\partial \bar{T}}{\partial x_j}, \frac{\partial \rho}{\partial x_j}, \text{Pr}, y^*) \quad (16)$$

In the above,  $S_{ij}$  and  $W_{ij}$  are, respectively, the mean rate of strain and mean vorticity tensors:

$$S_{ij} = \frac{1}{2} \left( \frac{\partial \bar{u}_i}{\partial x_j} + \frac{\partial \bar{u}_j}{\partial x_i} \right) \quad (17)$$

$$W_{ij} = \frac{1}{2} \left( \frac{\partial \bar{u}_i}{\partial x_j} - \frac{\partial \bar{u}_j}{\partial x_i} \right) \quad (18)$$

Fig. 10.  $Bo^*$  and  $Kv$  number for all the cases.

For the moment we confine our attention to our learning targets, considering the case of supercritical pressure flow with buoyancy and thermal acceleration effects. Considering the definition in Eq. (11), the functional form of ML targets has been derived by dimensionalizing the constitutive relation under the basic relationship of turbulent shear stress and heat flux see Eqs. (15) and (16). The ML target can eventually be written as a function of dimensionless features:

$$\begin{aligned} P_k^h &= f_{pk}(q_1, q_2, \dots), G_k^h = f_{gk}(g_1, g_2, \dots) \\ v_t^h &= f_{vt}(q_1, q_2, \dots), \kappa_t^h = f_{kt}(g_1, g_2, \dots) \end{aligned} \quad (11)$$

where  $\{q_1, q_2, \dots\}, \{g_1, g_2, \dots\}$  consists of all possible invariants of the relevant tensor variables listed in Eqs. (15) and (16), respectively. Note that, to ensure that the model does not depend on any specific types of flow, the features should be defined as a dimensionless combination of local flow variables rather than macro quantities.

For the practical computation of turbulent flows, it is no necessary to retain all terms in Eqs. (15) and (16) for the model to

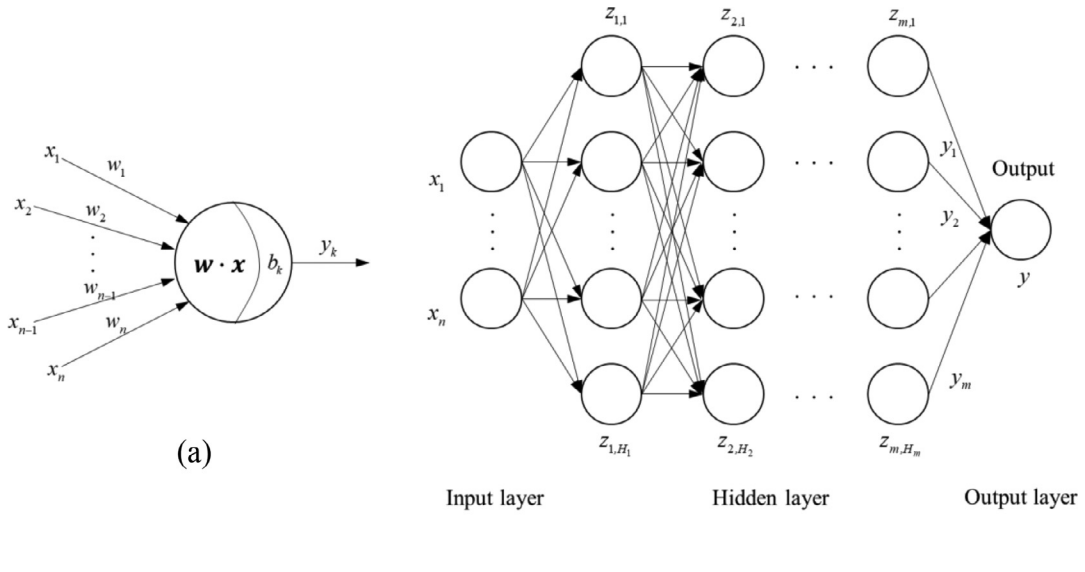


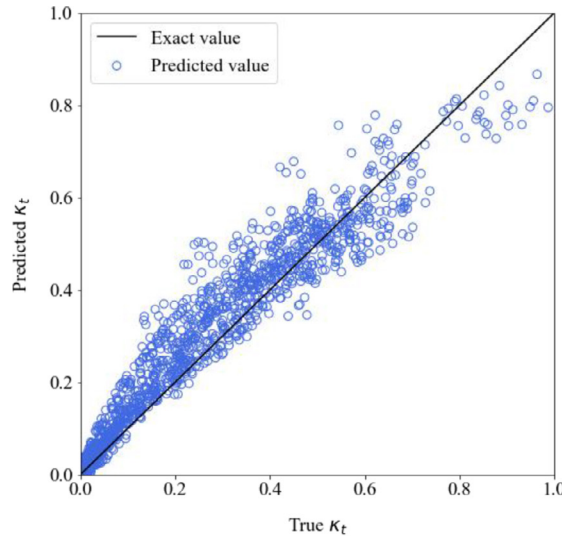
Fig. 9. The diagram of neuron and deep neural network model.

remain rational. For a ML algorithm, a good learning sample is the key to training the model. Selecting N features from the existing M features to optimize specific indicators of the system is an important method to improve the performance of the learning algorithm and significant Data Pre-processing steps in pattern recognition. The validity of a simplified set of features will obviously depend on the prior knowledge and feature selection method invoked. By combining the filtering approach with the packaging approach, we can build the feature set from the bottom up based on the basic

set of features selected by the physic knowledge. Features are progressively added according to the order of recognition of individual features, and utility is tested by verifying that group output errors are reduced.

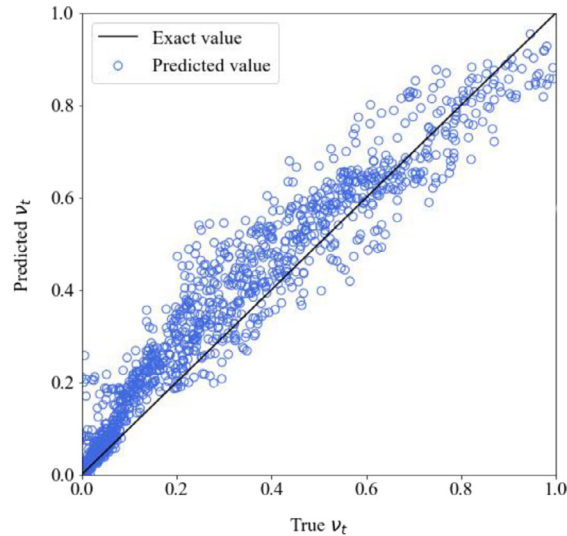
#### 2.4. Machine learning

Deep neural networks are used to construct regression models of the learning targets. Inspired by biological neural networks, the



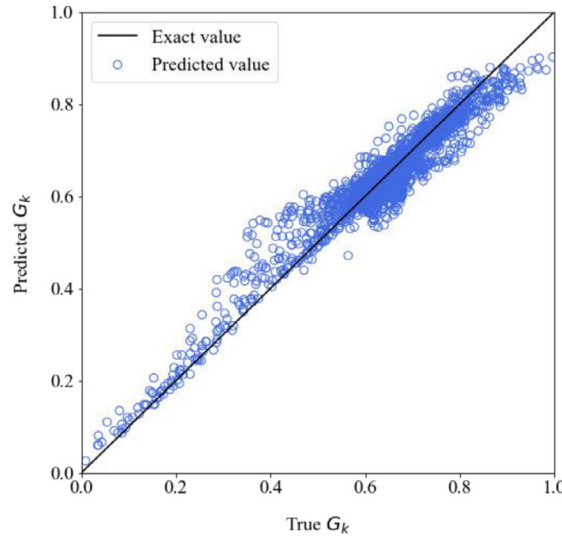
MSE=1.10e-2, Relative error =7.51%

(a)



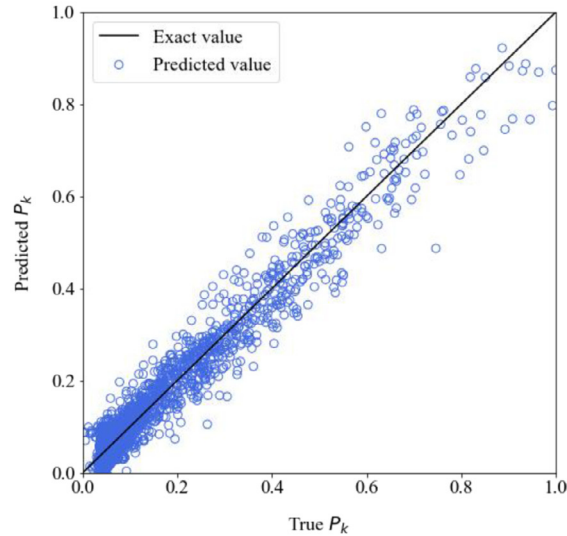
MSE=1.46e-2, Relative error =9.81%

(b)



MSE=2.23e-2, Relative error =3.72%

(c)



MSE=5.17e-3, Relative error =3.47%

(d)

**Fig. 11.** Performance of the validation set by the DNN at the end of the training phase.

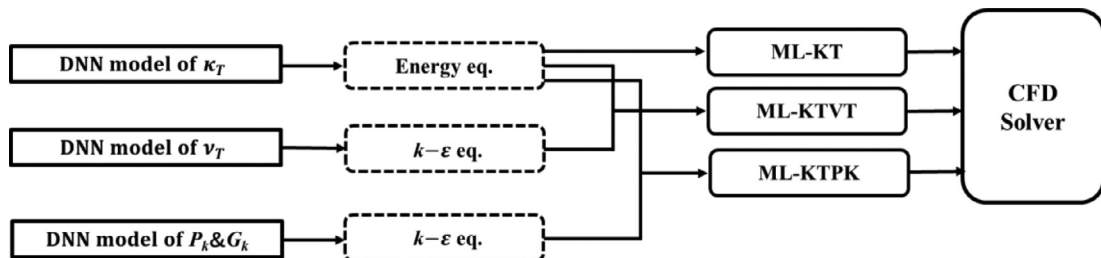


**Fig. 12.** Workflow of the built-in solution of three ML-based models. (I) ML-KT model. (II) ML-KTVT model. (III) ML-KTPK model.

**Table 2**  
Database for model training.

Cases	References	Fluid	P (Mpa)	G <sub>b</sub> (kg/m <sup>2</sup> s)	D(mm)	q <sub>w</sub> (kW/m <sup>2</sup> )	Datasize
#1	Yan et al. [55]	CO <sub>2</sub>	7.6	253.13	1	27	1835
#2						48	1782
#3						63	1800
#4	Cao et al. [39]	CO <sub>2</sub>	7.75	236.96	1	78	2728
#5	Bae et al. [29]	CO <sub>2</sub>	8.0	166.62	2	30.87	1965
#6				333.24	1	61.74	1910

**Table 3**  
Network configuration and hyperparameters.

Hyperparameters	Recommend Values for $\kappa_T$ model	Recommend Values for $\nu_T$ model	Recommend Values for $G_k$ model	Recommend Values for $P_k$ model
Hidden units	[50,30]	[120,120,120]	[50,30]	[85,85,85]
Activation function	ReLU	Leaky_ReLU	ReLU	ReLU
Optimizer	RMSPropOptimizer	AdamOptimizer	RMSPropOptimizer	RMSPropOptimizer
Learning rate	0.001	0.001	0.001	0.001
Batch size	1000	1500	500	500
Loss function	MSE	MSE	MSE	MSE
Max steps	15000	15000	10000	10000

artificial neural networks system is a highly complicated nonlinear kinetics system. They can have different architectures and properties of their processing elements. Fig. 9(a) is a diagram of a simple artificial neuron model, in which neurons receive signals transmitted from other neurons,  $x_1, x_2, \dots, x_n$ , these input signals are connected through the weights  $w_1, w_2, \dots, w_n$ , the results are compared

with the threshold  $b_k$ , and then processed by the activation function to obtain the output of neuron from.

The network structure used in this study is shown in Fig. 9(b), which includes the input layer, hidden layer and output layer. As can be seen from the figure, the number of nodes in the network input layer is  $n$ , the number of nodes in the hidden layer is

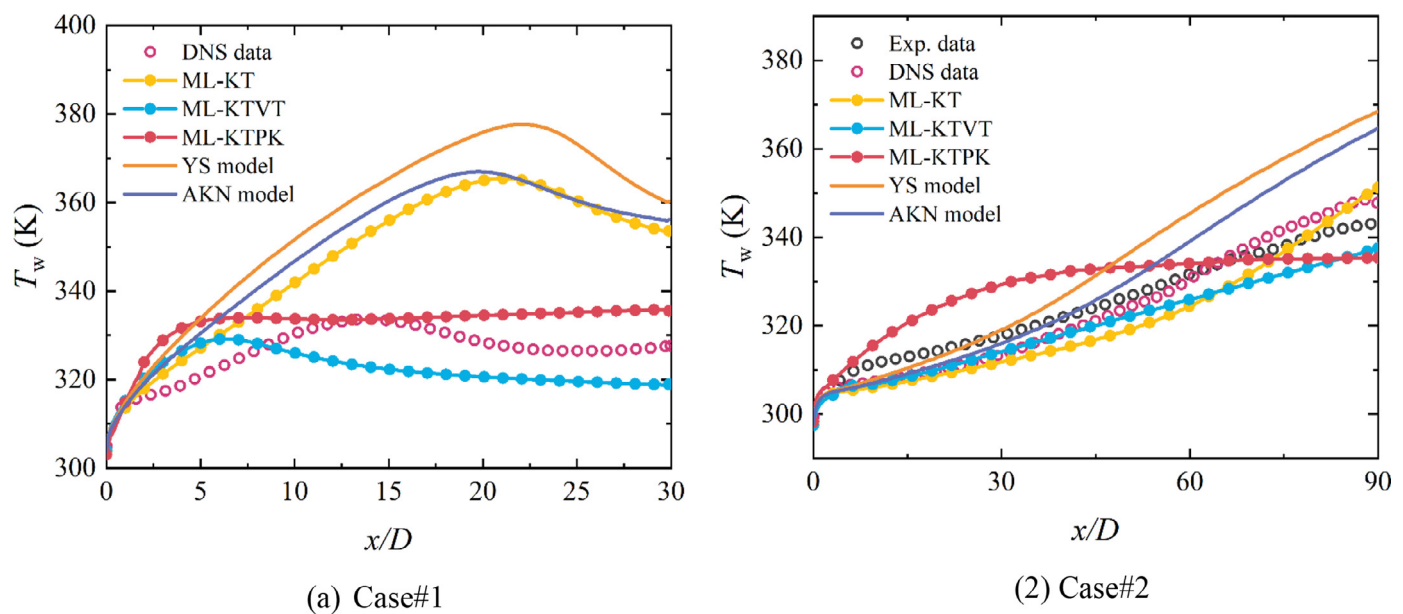


**Fig. 13.** Comparison of measured and predicted wall temperatures.

$H_1, H_2, \dots, H_m$  and the number of nodes in the output layer is 1. For a given training set  $D = \{(x_1, y_1), (x_2, y_2), \dots, (x_p, y_p)\}$ ,  $x_i \in \mathbb{R}^d$ ,  $y_i \in \mathbb{R}^1$ , the input set is  $d$  dimensional, the output set is 1 dimensional, and the output of the first hidden layer is  $z_{1,1}, z_{1,2}, \dots, z_{1,H}$ , where the input of  $z_{1,j}$  is  $x_1, x_2, \dots, x_n$ ,

$$z_{1,j} = f_1 \left( \sum_{i=1}^n w_{ij}^{(1)} x_i \right) \quad (12)$$

where  $f_1$  and  $w_{ij}^{(1)}$  is activation function and threshold of the first hidden layer, respectively.

The output of the second hidden layer is  $z_{2,1}, z_{2,2}, \dots, z_{2,H}$ , where the input of  $z_{2,i}$  is the output of the first hidden layer  $z_{1,1}, z_{1,2}, \dots, z_{1,H}$ ,

$$z_{2,j} = f_2 \left( \sum_{i=1}^{H_1} w_{ij}^{(2)} z_{1,i} \right) \quad (13)$$

The output of the network is:

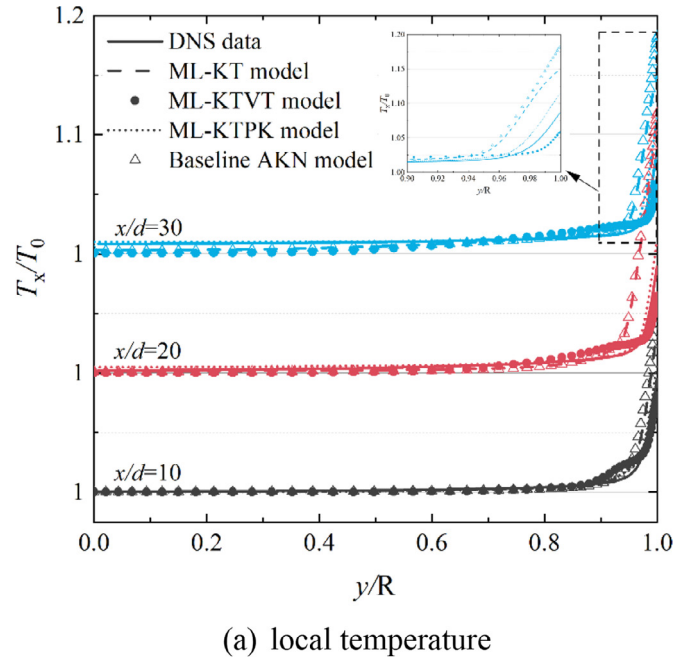
$$y = f_{m+1} \left( \sum_{i=1}^{H_m} w_{ij}^{(m+1)} z_{m,i} \right) \quad (14)$$

### 3. Results and discussion

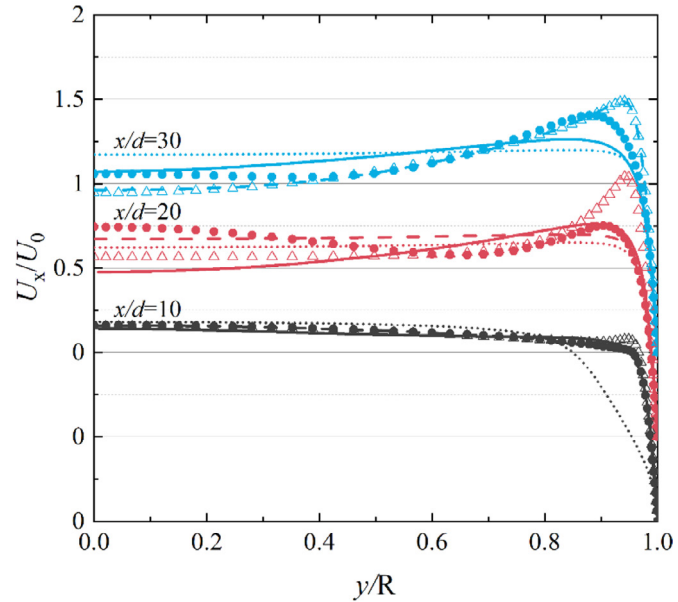
In this section, DNNs are trained using DNS data from heated turbulent flows flowing upward in vertical tubes at supercritical pressure. The DNS data from Bae et al. [29], Yan et al. [55] and Cao et al. [39] are used as the learning dataset, with the diameter of the fluid domain between 1 and 2 mm and the working fluid being carbon dioxide. In the training process, the original dataset is divided into the training and validation data with StratifiedShuffle-Split from scikit-learn. StratifiedShuffleSplit is a stratified sampling method, which returns stratified splits, i.e. which creates splits by preserving the same percentage for each target class as in the complete set. The training data are used by the optimization algorithms to adjust weights in the DNN, whereas the validation data are used to monitor and control the training process by adjusting the hyperparameters such as the structure of the DNN and learning rate. Then, the well-trained ML-RANS models are first tested with the same case as the training cases to verify the reproducibility of the training data, and at bulk parameters distributed within the range of training data to assess the generalization ability. Furthermore, the models are tested in cases with large diameter and different working fluid to validate the predictive capability in a flow regime that deviates from the training cases. In addition, the performance of different ML-RANS models is analyzed based on the mechanism of flow heat transfer, and the possible improvement strategies of such a physical informed machine learning model are proposed.

#### 3.1. Training phase

Turbulent heat transfer of supercritical pressure fluids in vertical tubes has been investigated by many researchers with direct numerical simulation (DNS), which can provide a sufficient quantity of high-fidelity local data and details of thermal fluid for machine learning. There are 6 DNS cases selected to provide a credible database for the DNN, containing the typical flow and heat transfer phenomenon of SCP fluid. Details of the training and validation dataset are given in Table 2. Noted that all cases are in upward direction. The dimensionless coefficients  $Bo^*$  and  $Kv$  representing the effect of buoyancy and thermal acceleration are shown in Fig. 10. It can be seen that these working conditions basically reflect



(a) local temperature



(b) local velocity

Fig. 14. Local velocity and local temperature in Case#1.

the coupling influence of buoyancy and flow acceleration. Considering the scope of the training data, the ML-RANS models based on that are suitable for predicting the upward pipe flows influenced by buoyancy effect ( $Bo^* < 2 \times 10^{-5}$ ) and the flows influenced by small flow acceleration ( $Kv < 2 \times 10^{-6}$ ). Noted that, some of the cases (Case #1,2,3,4) are validated by experimental results, which verify the reliability of the DNS data.

For the training of the ML models, Google's Tensorflow [59] machine learning framework is adopted for the construction of the DNNs. The ReLU [60] and Leaky\_ReLU [61] activation function have been used for the inner layers.

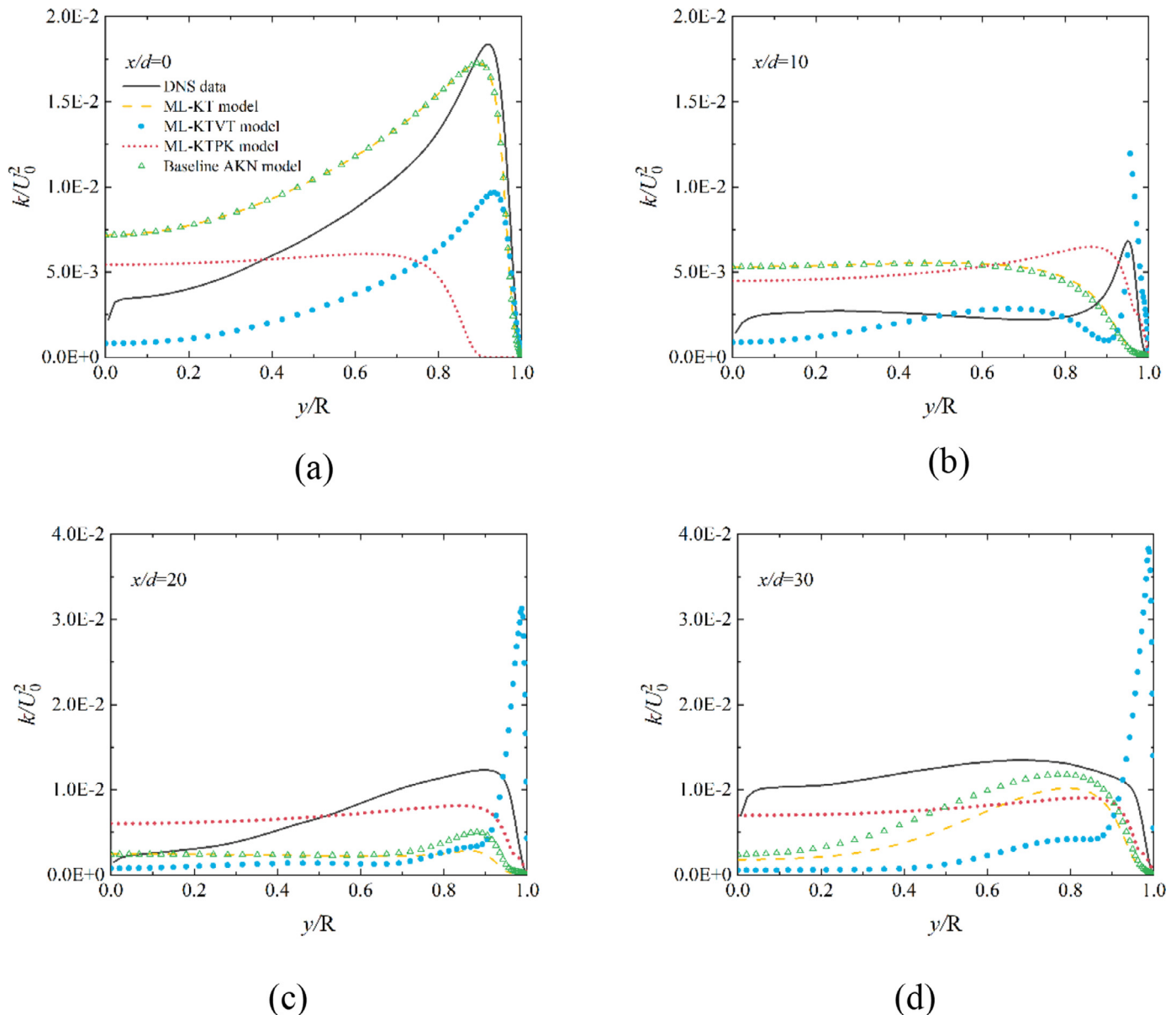


Fig. 15. Turbulent kinetic energy distributions for Case#1.

$$\text{ReLU function}$$

$$\text{ReLU}(x) = \begin{cases} x, & x > 0 \\ 0, & x \leq 0 \end{cases} \quad (15)$$

$$\text{Leaky_ReLU function}$$

$$\text{Leaky\_ReLU}(x) = \begin{cases} x, & x > 0 \\ 0.01x, & x \leq 0 \end{cases} \quad (16)$$

The ReLU provides a faster optimization in our case, which is also the most often used activation function in NN. However, there comes a dead ReLU problem in the NN model for eddy viscosity, Leaky\_ReLU which allows for negative activations is believed to solve this problem to some extent. The output activation function is linear, and the network training is performed with back-propagating errors. A z-score normalization is applied to the training set. The magnitude of mean square error (MSE) of the validation data is used to evaluate the training error. At the end of the training, the error of the validation data converges to the lowest

level, indicating that the ML model is not over-fitted in the training process. Several network configurations have been tested, starting from 5 layers of 100 neurons. The final network configuration and hyperparameters are listed in Table 3.

The a priori result of four learning targets is presented in Fig. 11. It can be seen that the four variables all achieved a satisfactory result in the validation dataset. However, we can see that the performance of the eddy diffusivity and eddy viscosity model is less perfect than the other two variables. That's because at the near-wall and tube center, there exist regions where the gradient of temperature or velocity vanishes or crosses the zero, which leads to violent singularity in eddy diffusivity and eddy viscosity (Eq. (11)). In this case, part of the reference data had to be removed from the regions where the coefficients reach very strange values. And an empirical damping function  $f = \sqrt{1 - \exp(-y^*/A^*)}$  is used to account for the strong nonlinear behavior of eddy diffusivity and eddy viscosity near the wall, the value of  $A^*$  was set as 10.

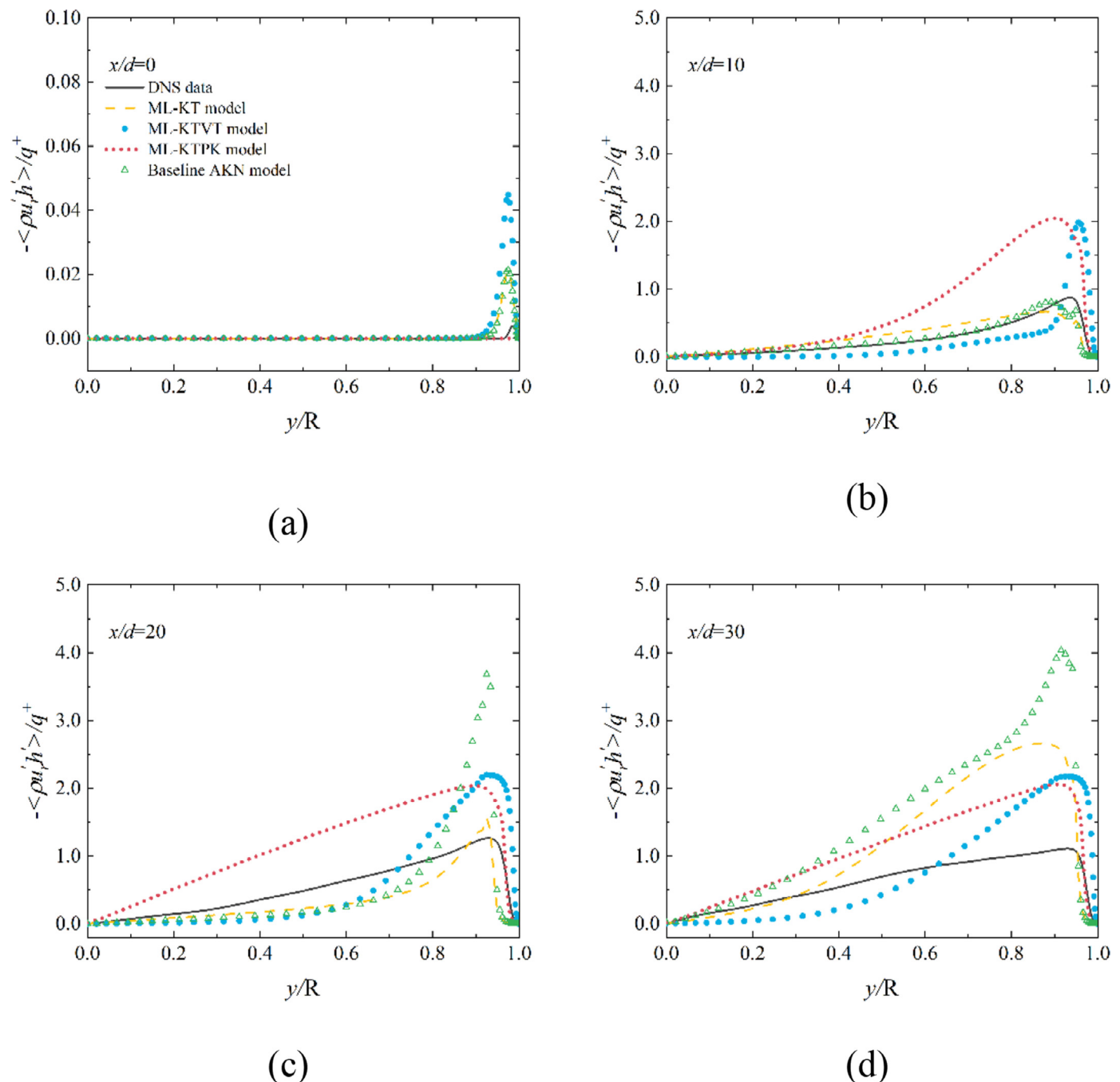


Fig. 16. Radial turbulent heat flux distributions for Case#1.

### 3.2. Predicting phase

#### 3.2.1. Numerical method

With the model trained, the weights and bias of each layer in the DNN are frozen and are available for numerical implementation in the form of explicit expression. In the predicting phase, the DNN model in the frozen Tensorflow graph is implemented in ANSYS FLUENT® CFD software package [ANSYS FLUENT 19.2.0, ANSYS FLUENT Inc., 2016] using User-Defined Functions (UDF) to reproduce precisely the numerical results obtained with the in-built ML-RANS turbulence model at each iterative step. The SIMPLEC scheme was used to couple the pressure and velocity fields. The QUICK scheme is used for spatial discretisation of the momentum equation and the UPWIND scheme is used for other equations.

The fluid thermal properties were calculated based on the NIST Standard Reference Database 23(REFPROP) [3] database, and integrated into Ansys Fluent using a piecewise-linear function through the user-defined database. Structured rectangular grids are used in the calculation, the mesh was refined in the radial direction and the axial direction at the position where heating commenced, and the dimensionless wall distance  $y^+$  at the first node from the wall was always far less than 1. The convergence criterion for the normalized residual of each equation was set to be less than  $10^{-6}$ .

To establish the in-built ML-RANS model, the DNN models are embedded with the baseline AKN model (see Section 2.2) by writing a user interface program (UDF) in C language. While embedding the DNN models in the CFD solver, we packaged the buoyancy production term  $G_k$  and the Reynolds stress production term

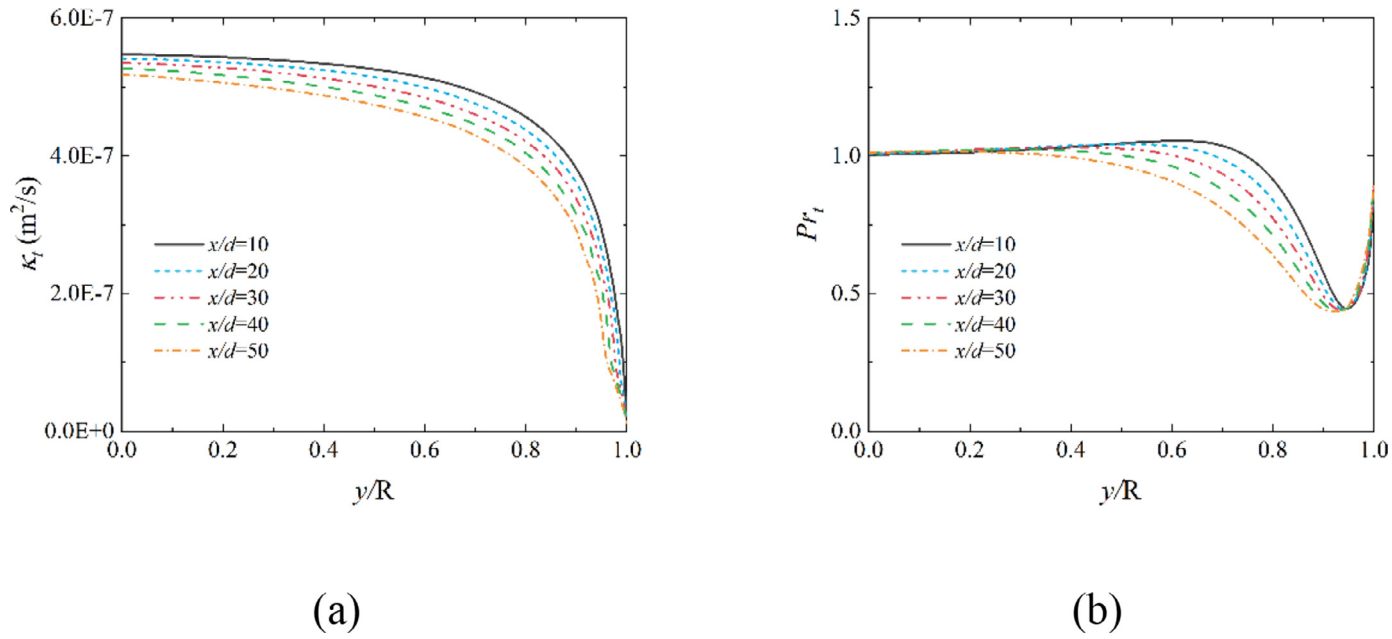


**Fig. 17.** The eddy diffusivity and turbulent Prandtl number  $Pr_t$  for Case#2.

**Table 4**  
List of posterior test cases.

Cases	Refs.	Fluid	P(Mpa)	$G_b(\text{kg}/\text{m}^2\text{s})$	D(mm)	$q_w (\text{kW}/\text{m}^2)$	$T_{in}(\text{K})$	Data source
#1	Bae et al. [29]	$\text{CO}_2$	8.0	166.62	2	30.87	301.15	DNS
#2	Xu et al. [63], Yan et al. [55]	$\text{CO}_2$	7.6	253.13	1	27	297.15	EXP & DNS
#3	Wang et al. [64], Cao et al. [39]	$\text{CO}_2$	7.75	236.96	1	49	296.15	EXP & DNS
#4	Fewster [65]	$\text{CO}_2$	7.58	636	5	64	293.88	EXP
#5	Pis'menny [66]	$\text{H}_2\text{O}$	23.5	248	6.28	276	473.15	EXP
#6	Gu et al. [56]	$\text{H}_2\text{O}$	23.0	1000	10	700	576.15	EXP
#7	Wang et al. [64], Cao et al. [39] (downward flow)	$\text{CO}_2$	7.75	236.96	1	49	296.15	EXP & DNS

$P_k$  into one production term. Define the combination production term  $\mathcal{P}_k$  as

$$\mathcal{P}_k = P_k + G_k = -\overline{\rho u_i' u_j''} \frac{\partial \bar{u}_i}{\partial x_j} \mp \frac{g R^*}{U_0^2} \overline{\rho' u_x'}$$

By embedding the algebraic models into the energy and  $k-\varepsilon$  equations in the baseline AKN model, the computational framework provides an iterative solution to improve the performance of the RANS solver. Through the combination of DNN models respectively, several turbulence models can be obtained, we list them as follows to distinguish the single or composite models in the remainder of this article. There are three combination models refer to return only eddy diffusivity field (I), eddy diffusivity and eddy viscosity field (II) or eddy diffusivity and the combined production field (III) to the CFD solver.

To give an assessment of the performance of the DNN based models, we have selected some classical low-Reynold number  $k-\varepsilon$  models for comparison: Abe, Kondoh and Nagano (AKN) [5], and Yang-Shih (YS) [62]. For the posterior test of the model, experimental and high-fidelity numerical simulation cases were used to test the performance of the ML-RANS model, wherein Group 1 (Case#1 #2) was included in the machine learning data set, while Group 2 (Case#3 #4 #5 #6 #7) were not. Noted that case#7 is selected to examine the applicability of the modified model in downward vertical flows, the other are all upward flows. Details of the test cases are given in Table 4. All test cases are in upward direction.

### 3.2.2. Validation with cases within the training set

The results of training cases are reported in Fig. 13. The heat transfer deterioration and recovery process are of significance for

designing supercritical fluid applications, so as the performance of the thermal fluid model. It can be seen that the wall temperature was better predicted using the composite ML-RANS model (ML-KTVT and ML-KTPK) than the single ML-KT model and original LRN models. The deterioration of heat transfer is greatly exaggerated or underestimated by the LAS, YS and original AKN model. The ML-KT model reduced the overestimation of heat transfer deterioration to some degree, however, the model still could not capture the exact position and magnitude of the wall temperature peak. The ML-KTPK model accurately captured the highest temperature deterioration value, but the location of deterioration was early predicted and the temperature valley was not predicted. It can be concluded from the following analysis that it was unable to predict the wall temperature valley where the heat transfer enhancement occurs. It is shown that the results calculated by the ML-KTVT demonstrated the most reasonable agreement with the experiment and DNS data, the distance between the position of the calculated temperature peak and the one observed in DNS data was less than 10 D, and the difference of the wall temperature peak between the calculated results with DNS data is less than 12 K.

More detailed information on flow heat transfer is adopted to verify the performance of the model. The DNS cases by Bae et al. [29] were adopted to evaluate the applicability of the ML-RANS model for reproducing the reasonable flow and thermal field. It's a typical turbulent heat transfer case containing heat transfer deterioration and a recovery process dominated by buoyancy effects. Fig. 14 demonstrates the comparison of the local temperature and streamwise velocity by the original AKN model and the ML-RANS model with the DNS data. The local velocity and local temperature field predicted by the ML-KTVT model are very close to the DNS

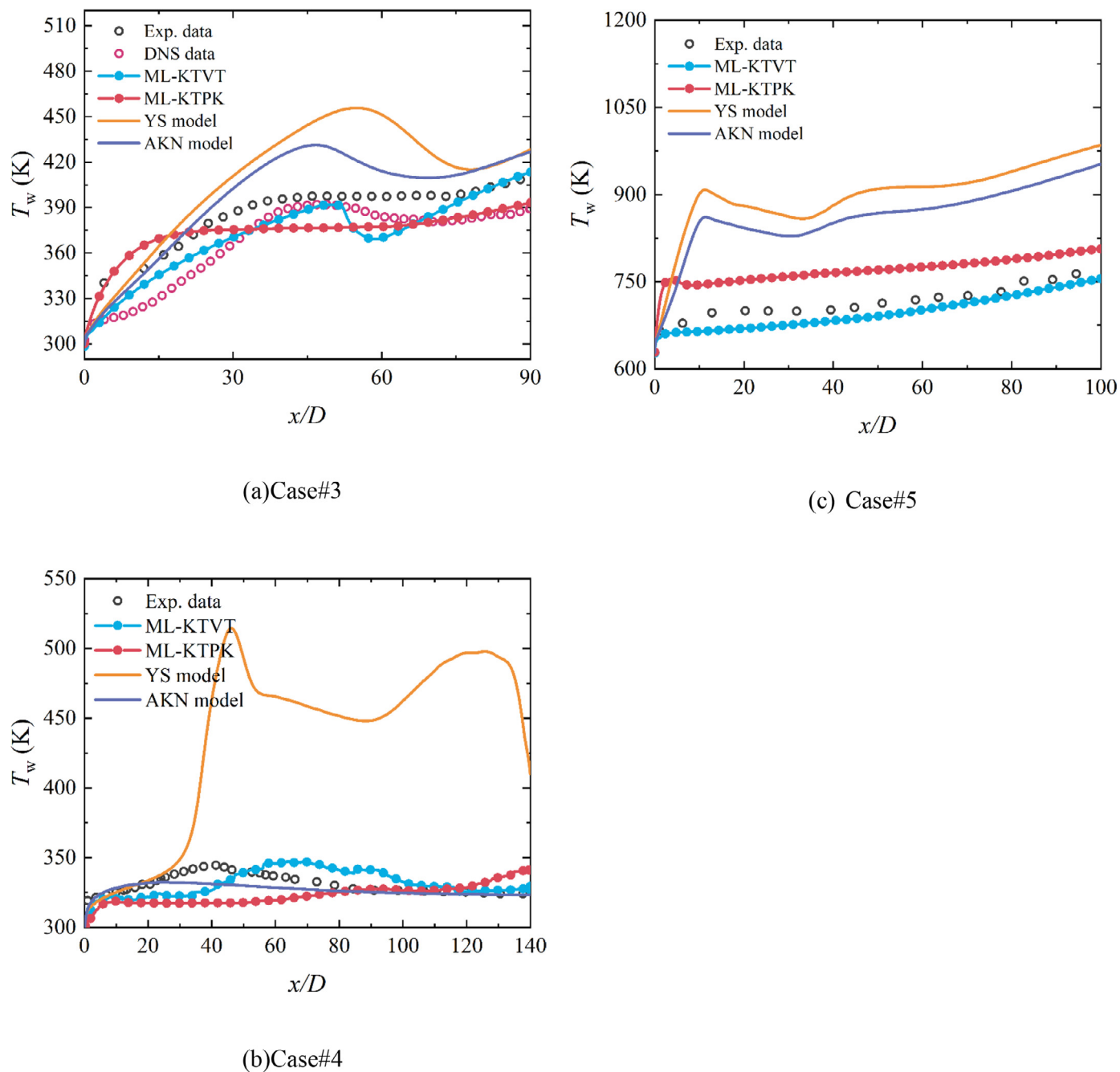
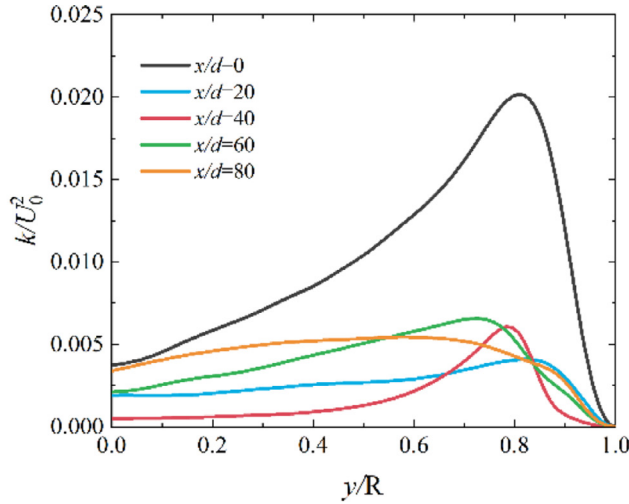


**Fig. 18.** Comparison of measured and predicted wall temperatures.

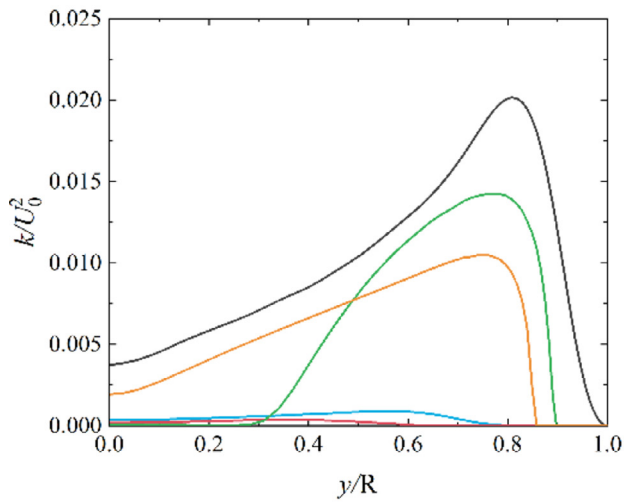
data. As shown in Fig. 14(a), because of the heated fluid in the near-wall region across the pseudocritical point, the large density difference across the flow field developed a strong upward buoyancy force, which contributed to the streamwise velocity acceleration near the wall. In upward flow where the buoyancy-induced flow acceleration and the forced flow occur in the same direction, the velocity profile becomes flattened at the location of  $x/D=10$ , and to “M-shaped” at the location at  $x/D=20$  and 30. The flattened velocity profile caused decreased radial gradient of velocity, and the production of turbulent kinetic energy due to shear stress, which is associated with the velocity profile, appears to attenuate at the location where the flattened velocity profile occurs. Therefore, localized heat transfer deterioration occurs as the result of turbulence attenuation. Whereas, the following “M-shape” velocity profile contributes to the recovery of turbulence and heat trans-

fer. The ML-KTVT model accurately predicted the distorted velocity profiles by the buoyancy effect. The original AKN model predicted the “M-shaped” velocity profile early than the DNS result, while the ML-KT model later. But the performance of the ML-KTPK model is not satisfactory, since it could only reproduce the flat velocity distribution but not the following “M-Shaped” velocity profile.

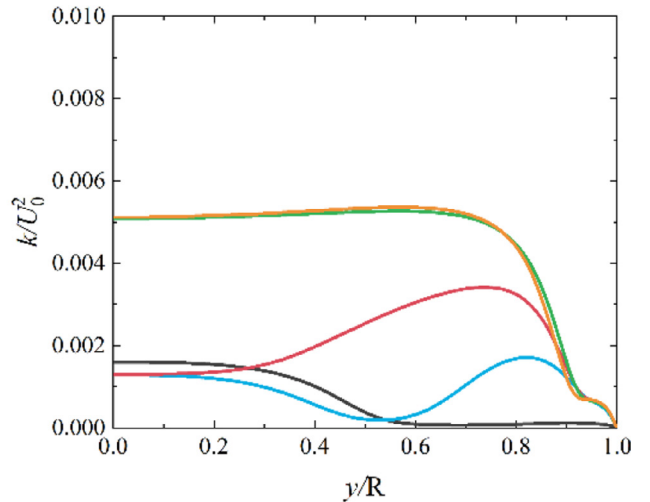
Advanced calculation of turbulent kinetic energy and turbulent heat flux is important for better evaluations of turbulent heat transfer due to the buoyancy effect. As explained in the previous sections, some of the important turbulent statistics are associated with the strong buoyancy effect. Fig. 15 shows the distributions of the turbulent kinetic energy for Case#1. By doing so, we have a direct picture of turbulence energetics and heat transfer deterioration due to the buoyancy effect. In the present discussion, turbu-



(a)DNS data



(d) ML-KTVT model



(c)ML-KTPK model

**Fig. 19.** The comparison between the predictions of the ML-KTVT model and ML-KTPK model and the DNS of profiles of TKE for Case#3.

lence kinetic energy (TKE)  $k = \frac{1}{2} \widetilde{u_i'' u_i''}$  is mainly concerned to describe the development of the flow. As we can see from Fig. 15, the TKE is high at the inlet but decreases to about one-half of the corresponding inlet values at  $x/D=10$  in DNS results, where the buoyancy-induced flow motion appears flattened velocity distribution in Fig. 13. Such a reduction in turbulence results in a severe wall temperature increases at  $x/D=0-10$ . At downstream  $x/D=20$  the mean velocity profile is deformed into an “M-shaped” profile, the TKE distribution increase according to the double production peaks in the buffer layer (not shown here). Near the end of the heated tube at  $x/D=30$ , the TKE is transported to the core re-

gion by convection and diffusion term, and therefore the turbulent heat transfer recovered to a high level. The modified models demonstrate different abilities in predicting the turbulence development, the ML-KT model and the original AKN model can qualitatively capture the overall trend of the turbulence attenuation. But the worst point was greatly exaggerated, and the location where heat transfer recovery occurs is delayed. The ML-KTVT model can capture both deterioration and recovery of the TKE especially in the near-wall region. It's also noteworthy that the distribution of TKE in the core region in the ML-KTVT model is always lower than the DNS results meanwhile the peak of TKE in the vicinity of the

**Table 5**

The time cost of calculation for Case#1 [29].

Model	Time cost
Baseline AKN	3min 9s
MK-KT	2min 51s
ML-KTVT	2min 32s
ML-KTPK	2min 05s

tube wall is much higher than the DNS results, which might be attributed to the unreasonable distribution of velocity at the core region (Fig. 14). The machine learning model has not learned how to correct this false shape of velocity profile yet.

Fig. 16 shows the distributions of the radial turbulent heat flux  $-\rho u''_r h''/q^+$  for Case#1, in which the  $q^+ = \frac{q_w}{\rho_0 U_0 c_p T_0}$  is the nondimensional heat flux used to normalize the turbulent heat flux. Due to the turbulence attenuation, the magnitude of radial turbulent heat flux is smaller at  $x/D=10$  and then grows to a normal level in farther downstream region. This explains why the centerline temperature in Fig. 13 developed slowly. All models in this work could reproduce the overall trend, the ML-KTVT model demonstrated more reasonable agreement with the DNS data.

An analysis of time cost of calculation is also performed. Due to different hardware and computational configuration, the absolute running time of a solver may differ, but the comparison of the computation time to a traditional model within the same configuration is still informative. Table 5 shows the time cost of one calculation for Case#1 from beginning to total convergence. The ML-RANS model is lighter than the original AKN model with the time cost being much lower. Consequently, under the same convergence conditions, applying the algebra DNN model can considerably reduce the computation cost.

It is worthwhile to mention here that although the single ML-KT model and ML-KTPK model didn't perform as well as the ML-KTVT model for Case#1, they could still reduce the overestimation of heat transfer deterioration to some extent than all the LRN models considered in this work. Some considerable results have been obtained in Case#2. Fig. 17 shows the eddy diffusivity and turbulent Prandtl number  $Pr_t$  for Case#2. It's clear that the turbulent Prandtl number  $Pr_t$  in the ML-KT model is less than the constant value  $Pr_t=0.85$  used by the common LRN model in buffer later. The over-estimate in common LRN models might have resulted either from an incorrect turbulence model or from an unrealistic treatment of the turbulent Prandtl number as a constant. Obviously, the modified  $Pr_t$  calculated by the DNN model is more reasonable for supercritical fluids than the constant value.

### 3.2.3. Validation with generalization cases

To further evaluate the robustness and generalization capability of the developed ML-RANS model, the ML-RANS model is further tested in Case#3-#5, to examine the performance of the model in an interpolation heat flux, a larger tube and a different type of fluid, respectively. Fig. 18 shows the distribution of the wall temperature in the three cases predicted by various turbulence models compared with DNS and experimental results. According to the analysis before, the ML-KT model is believed to basically improve the model performance, so in this section we only adopt the ML-KTVT and ML-KTPK models for comparation. It can be observed that the YS model consistently over-predicts the wall temperature for each case. The AKN models underestimate the wall temperature for some cases but over-predict it for the other case. The ML-KTVT model appears to produce the best prediction of wall temperature among all the models tested, whereas HTD predicted by the ML-KTPK model always occurs at the inlet and recovered progressively in the downstream direction. The wall temperature in the ML-KTPK model is continuously increasing in the streamwise direction. It is

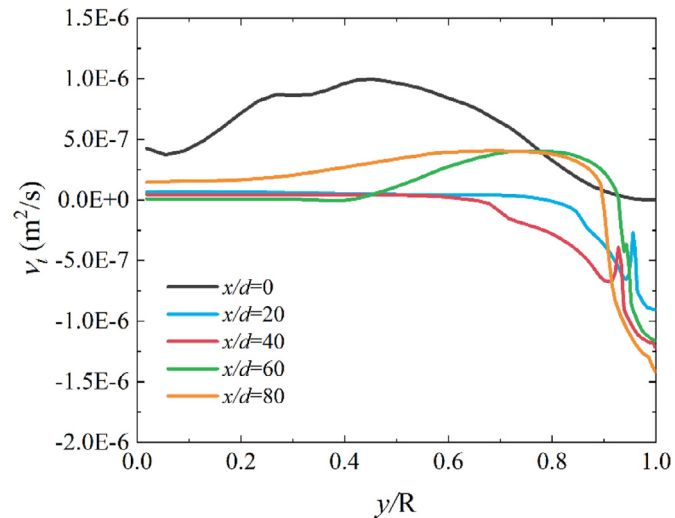


Fig. 20. The eddy viscosity predicted by the ML-KTVT model for Case#3.

of interest to note that the ML-KTVT model still performs better than all LRN models used in this work in heat transfer prediction of supercritical water in a large diameter tube, even though there is no such information in the machine learning dataset. The result indicates a promising further development and application of the ML-based thermal fluid model.

From the former study [39], we know that Case#3 is under the coupling effects of strong buoyancy and thermal acceleration, in which the turbulence production and TKE appear the developing periods as 'decrease-regenerate-decrease'. In this progress, the flow is dominated by buoyancy at the very first, driving the mean velocity profile to be flattened after the start of heating, followed by further distortions downstream becoming an inverted M-shaped distribution. Turbulence production reduces initially, but as the velocity turns into an M-shape TKE increases again. After that under the control of thermal acceleration, the turbulence flow attenuation happens again. Fig. 19 shows the development of TKE predicted by different models and DNS for Case#3. Both two ML-RANS models reproduce the flow re-laminarization at the very beginning of the heated flow, but their detailed predictions differ significantly from the DNS results.

Therefore, the wall temperature in forced convection of supercritical flow becomes higher progressively. The ML-KTVT model under-predicted the turbulence strength as the heat transfer deteriorated, where the TKE nearly completely diminished, but it surprisingly recovered to a significant magnitude at  $x/D=60$ . This contributes to the successful picture on the strong recovery of heat transfer due to strong buoyancy effects. What's more, the ML-KTVT model also reproduces the second decrease in TKE caused by thermal acceleration, indicating that the different mechanisms of buoyancy and thermal acceleration influencing the turbulent heat transfer can be distinguished and learned in the present framework. However, the ML-KTPK model responded too early to the effect of buoyancy and was not able to reproduce a reasonable degree of recovery. Consequently, the ML-KTPK model performs in a similar manner in the current study, predicting the temperature curve that deteriorates and then increases linearly.

A closer inspection of the eddy viscosity results with the ML-KTVT model shows that the machine learning model could accurately predicted the turning point that exists in the DNS results (see Fig. 6). This contributes to the reproducibility of correct Reynolds stress so as the shear stress production. The performance of the present model does not perfectly agree with the DNS data, this might be due to some limitations in the modified model such

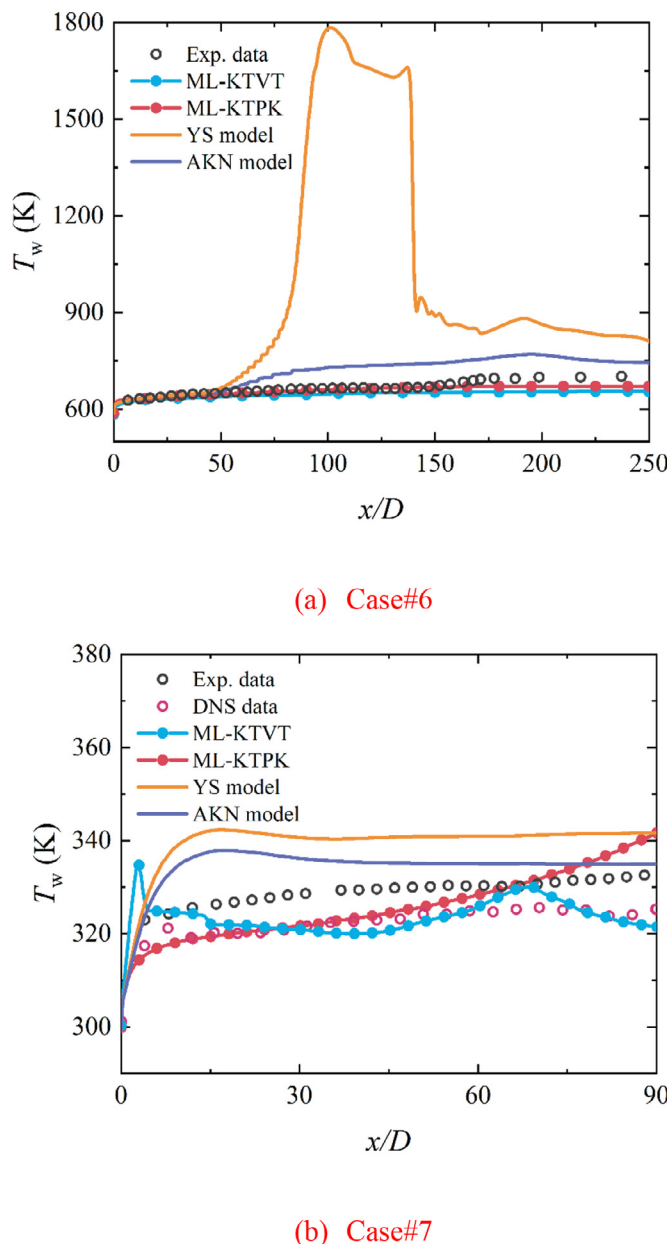


**Fig. 21.** Comparison of measured and predicted wall temperatures.

as eddy diffusivity isotropy assumed implemented in the energy equation and the original eddy viscosity model used in the momentum equation. It's still a promising method for future improvement in turbulence modeling of supercritical pressure fluid.

To further evaluate the applicability of the ML-RANS models, the comparisons of the original LRN models and the modified models with experimental and DNS data in larger diameter tube(case#6) and downward flow(case#7) are shown in Fig. 21. It's worthy to note that the flow condition is beyond the confines of the learning dataset. It is shown that the original YS and AKN model overestimates the heat transfer deterioration in case#6 and #7, while the results calculated by the ML-KTVT model demonstrated more reasonable agreement with the experimental data. Furthermore, it is noticed that the ML-RANS models present better stability and robustness than YS model. However, the accuracy of the prediction for downward flows still needs to be improved quantitatively. This could be attributed to the limitation of training data, leading to inaccuracy while migrate the underlying mecha-

nism to a wider range of operating conditions. The accuracy of ML model training process directly affects the effectiveness of the CFD solver, so it is of great significance to further improve the features, datasets as well as the machine learning algorithm. This paper provides a potential methodology for improving turbulent convection heat transfer model at supercritical pressure.

#### 4. Conclusions

In this work, a physics-informed machine learning based RANS turbulence model is developed for supercritical pressure fluid. Firstly, we discuss the challenges of applying machine learning techniques in a fluid dynamic setting and possible successful approaches. Furthermore, we established a DNS-DNN-RANS framework to construct an in-built turbulence model based on big data and prior knowledge. Moreover, several DNN regression models are developed and implemented into the CFD solver, three ML-RANS models are constructed and verified on five different cases within and without the range of the training data. The validation results show that the ML-KT model is better than the unrealistic constant  $\Pr_t$  hypothesis and the ML-KTVT model not only achieves a good reproducibility of the training cases but also performs a favorable generalization capability. This work explores the potential for machine learning as an enhancement to or replacement for traditional turbulence models. Our results highlight the potential and viability of machine learning approaches to aid turbulence model development.

It is worthwhile to mention that the AKN  $k-\varepsilon$  model has been the baseline model in the current study. However, the "DNS-DNN-RANS" framework supports portability to other turbulence models. Further advanced models are still being developed, including expanding more sophisticated databases to cover the complex mechanisms for closure terms and a method to embed DNN with CFD-solver avoiding relying on assumptions.

#### Declaration of Competing Interest

The authors declare that they have no known competing financial interests or personal relationships that could have appeared to influence the work reported in this paper.

#### Data availability

Data will be made available on request.

#### Acknowledgment

This project was supported by the Key Project Fund from the National Natural Science Foundation of China (No. U21B2056).

#### References

- [1] P.X. Jiang, Y. Zhang, R.F. Shi, Experimental and numerical investigation of convection heat transfer of  $\text{CO}_2$  at supercritical pressures in a vertical mini-tube, *Int. J. Heat Mass Transf.* 51 (2008) 3052–3056.
- [2] P.X. Jiang, B. Liu, C.R. Zhao, F. Luo, Convection heat transfer of supercritical pressure carbon dioxide in a vertical micro tube from transition to turbulent flow regime, *Int. J. Heat Mass Transf.* 56 (2013) 741–749.
- [3] E.W. Lemmon, M.L. Huber, M.O. McLinden, NIST Standard Reference Database 23: Reference Fluid Thermodynamic and Transport Properties-REFPROP. 9.0 (2010) NSRDS.
- [4] Launder, B.E. and Sharma, B.I. 1974. Application of the energy-dissipation model of flow near a spinning disc.
- [5] K. Abe, T. Kondoh, Y. Nagano, A new turbulence model for predicting fluid flow and heat transfer in separating and reattaching flows—II. Thermal field calculations, *Int. J. Heat Mass Transf.* 38 (1995) 1467–1481.
- [6] H.K. Myong, N. Kasagi, New approach to the improvement of  $\kappa-\varepsilon$  turbulence model for wall-bounded shear flows, *JSME Int. J.* 33 (1990) 63–72.
- [7] S. He, W.S. Kim, J.H. Bae, Assessment of performance of turbulence models in predicting supercritical pressure heat transfer in a vertical tube, *Int. J. Heat Mass Transf.* 51 (2008) 4659–4675.

- [8] Q.L. Web, H.Y. Gu, Numerical simulation of heat transfer deterioration phenomenon in supercritical water through vertical tube, *Ann. Nucl. Energy* 37 (2010) 1272–1280.
- [9] A. Pucciarelli, I. Borroni, M. Sharabi, W. Ambrosini, Results of 4-equation turbulence models in the prediction of heat transfer to supercritical pressure fluids, *Nucl. Eng. Des.* 281 (2015) 5–14.
- [10] P. Spalart, S. Allmaras, A one-equation turbulence model for aerodynamic flows, in: Proceedings of the 30th Aerospace Sciences Meeting and Exhibit, 1992.
- [11] D.C. Wilcox, Formulation of the k-w turbulence model revisited, *AIAA J.* 46 (2008) 2823–2838.
- [12] F.R. Menter, Two-equation eddy-viscosity turbulence models for engineering applications, *AIAA J.* 32 (1994) 1598–1605.
- [13] Y.Y. Bae, A new formulation of variable turbulent Prandtl number for heat transfer to supercritical fluids, *Int. J. Heat Mass Transf.* 92 (2016) 792–806.
- [14] G. Tang, H. Shi, Y. Wu, J. Lu, Z. Li, Q. Liu, H. Zhang, A variable turbulent Prandtl number model for simulating supercritical pressure CO<sub>2</sub> heat transfer, *Int. J. Heat Mass Transf.* 102 (2016) 1082–1092.
- [15] R. Tian, X. Dai, D. Wang, L. Shi, Study of variable turbulent prandtl number model for heat transfer to supercritical fluids in vertical tubes, *J. Therm. Sci.* 27 (2018) 213–222.
- [16] X. Du, Z. Lv, X. Yu, M. Cao, J. Zhou, Y. Ren, Q. Qiu, X. Zhu, Heat transfer of supercritical CO<sub>2</sub> in vertical round tube: a considerate turbulent Prandtl number modification, *Energy* (2020) 192.
- [17] M. Mohseni, M. Bazargan, A new correlation for the turbulent prandtl number in upward rounded tubes in supercritical fluid flows, *J. Heat Transf.* (2016) 138.
- [18] S. Kenjereš, S.B. Gunarjo, K. Hanjalić, Contribution to elliptic relaxation modelling of turbulent natural and mixed convection, *Int. J. Heat Fluid Flow* 26 (2005) 569–586.
- [19] J. Xiong, X. Cheng, Turbulence modelling for supercritical pressure heat transfer in upward tube flow, *Nucl. Eng. Des.* 270 (2014) 249–258.
- [20] A. Pucciarelli, M. Sharabi, W. Ambrosini, Prediction of heat transfer to supercritical fluids by the use of Algebraic Heat Flux Models, *Nucl. Eng. Des.* 297 (2016) 257–266.
- [21] P.X. Jiang, Z.C. Wang, R.N. Xu, A modified buoyancy effect correction method on turbulent convection heat transfer of supercritical pressure fluid based on RANS model, *Int. J. Heat Mass Transf.* 127 (2018) 257–267.
- [22] S. Koshizuka, N. Takano, Y. Oka, Numerical analysis of deterioration phenomena in heat transfer to supercritical water, *Int. J. Heat Mass Transf.* 38 (1995) 3077~084.
- [23] S. He, S.W. Kim, P.X. Jiang, J.D. Jackson, Simulation of mixed convection heat transfer to carbon dioxide at supercritical pressure, *Int. J. Therm. Sci.* 44 (2004) 521–530 2005.
- [24] S. He, P.X. Jiang, Y.J. Xu, R.F. Shi, W.S. Kim, J.D. Jackson, A computational study of convection heat transfer to CO<sub>2</sub> at supercritical pressures in a vertical mini tube, *Int. J. Therm. Sci.* 44 (2005) 521–530.
- [25] C.R. Zhao, Z. Zhang, P.X. Jiang, H.L. Bo, Influence of various aspects of low Reynolds number k-ε turbulence models on predicting in-tube buoyancy affected heat transfer to supercritical pressure fluids, *Nucl. Eng. Des.* 313 (2017) 401–413.
- [26] M. Mohseni, M. Bazargan, The effect of the low Reynolds number k-ε turbulence models on simulation of the enhanced and deteriorated convective heat transfer to the supercritical fluid flows, *Heat Mass Transf.* 47 (2010) 609–619.
- [27] M. Mohseni, M. Bazargan, Modification of low Reynolds number k-ε turbulence models for applications in supercritical fluid flows, *Int. J. Therm. Sci.* 51 (2012) 51–62.
- [28] B.D. Tracey, K. Duraisamy, J.J. Alonso, A Machine Learning Strategy to Assist Turbulence Model Development, in: Proceedings of the 53rd AIAA Aerospace Sciences Meeting, 2015.
- [29] J.H. Bae, J.Y. Yoo, H. Choi, Direct numerical simulation of turbulent supercritical flows with heat transfer, *Phys. Fluids* 17 (2005) 465–380.
- [30] J.H. Bae, J.Y. Yoo, H. Choi, D.M. McEligot, Effects of large density variation on strongly heated internal air flows, *Phys. Fluids* 18 (2006).
- [31] J.H. Bae, J.Y. Yoo, D.M. McEligot, Direct numerical simulation of heated CO<sub>2</sub> flows at supercritical pressure in a vertical annulus at Re=8900, *Phys. Fluids* (2008) 20.
- [32] Petukhov, B.S., Polyakov, A.F. and Launder, B.E. 1988. Heat transfer in turbulent mixed convection.
- [33] H. Nemati, A. Patel, B.J. Boersma, R. Pecnik, Mean statistics of a heated turbulent pipe flow at supercritical pressure, *Int. J. Heat Mass Transf.* 83 (2015) 741–752.
- [34] H. Nemati, A. Patel, B.J. Boersma, R. Pecnik, The effect of thermal boundary conditions on forced convection heat transfer to fluids at supercritical pressure, *J. Fluid Mech.* 800 (2016) 531–556.
- [35] J.W.R. Peeters, R. Pecnik, M. Rohde, T.H.J.J. Van Der Hagen, B.J. Boersma, Turbulence attenuation in simultaneously heated and cooled annular flows at supercritical pressure, *J. Fluid Mech.* 799 (2016) 505–540.
- [36] J.W.R. Peeters, R. Pecnik, M. Rohde, T.H.J.J. Van Der Hagen, B.J. Boersma, Characteristics of turbulent heat transfer in an annulus at supercritical pressure, *Phys. Rev. Fluids* 2 (2017).
- [37] J. He, R. Tian, P.X. Jiang, S. He, Turbulence in a heated pipe at supercritical pressure, *J. Fluid Mech.* 920 (2021).
- [38] S. He, K. He, M. Sedighi, Laminarisation of flow at low Reynolds number due to streamwise body force, *J. Fluid Mech.* 809 (2016) 31–71.
- [39] Y.L. Cao, R.N. Xu, J.J. Yan, S. He, P.X. Jiang, Direct numerical simulation of convective heat transfer of supercritical pressure in a vertical tube with buoyancy and thermal acceleration effects, *J. Fluid Mech.* 927 (2021).
- [40] B. Ničeno, M. Sharabi, Large eddy simulation of turbulent heat transfer at supercritical pressures, *Nucl. Eng. Des.* 261 (2013) 44–55.
- [41] J.N. Kutz, Deep learning in fluid dynamics, *J. Fluid Mech.* 814 (2017) 1–4.
- [42] K. Duraisamy, G. Iaccarino, H. Xiao, Turbulence modeling in the age of data, *Annu. Rev. Fluid Mech.* 51 (2019) 357–377.
- [43] S.L. Brunton, J.L. Proctor, J.N. Kutz, Discovering governing equations from data by sparse identification of nonlinear dynamical systems, *Proc. Natl. Acad. Sci. U.S.A.* 113 (2016) 3932–3937.
- [44] K. Duraisamy, Z.J. Zhang, A.P. Singh, New approaches in turbulence and transition modeling using data-driven techniques, in: Proceedings of the 53rd AIAA Aerospace Sciences Meeting, 2015.
- [45] E.J. Parish, K. Duraisamy, A paradigm for data-driven predictive modeling using field inversion and machine learning, *J. Comput. Phys.* 305 (2016) 758–774.
- [46] J.R. Holland, J.D. Baeder, K. Duraisamy, Towards integrated field inversion and machine learning with embedded neural networks for RANS modeling, in: Proceedings of the AIAA Scitech 2019 Forum, 2019.
- [47] J. Weatheritt, R. Sandberg, A novel evolutionary algorithm applied to algebraic modifications of the RANS stress-strain relationship, *J. Comput. Phys.* (2016) 22–37.
- [48] H.D. Akolekar, J. Weatheritt, N. Hutchins, R. Sandberg, G.M. Laskowski, V. Michelassi, Development and use of machine-learnt algebraic reynolds stress models for enhanced prediction of wake mixing in LPTs, *J. Turbomach.* (2018).
- [49] J. Weatheritt, R.D. Sandberg, The development of algebraic stress models using a novel evolutionary algorithm, *Int. J. Heat Fluid Flow* 68 (2017) 298–318.
- [50] W. Liu, J. Fang, S. Rolfo, C. Moulinec, D.R. Emerson, An iterative machine-learning framework for RANS turbulence modeling, *Int. J. Heat Fluid Flow* (2021) 90.
- [51] J. Ling, A. Kurzawski, J. Templeton, Reynolds averaged turbulence modelling using deep neural networks with embedded invariance, *J. Fluid Mech.* 807 (2016) 155–166.
- [52] J. Ling, R. Jones, J. Templeton, Machine learning strategies for systems with invariance properties, *J. Comput. Phys.* 318 (2016) 22–35.
- [53] J.X. Wang, J.L. Wu, H. Xiao, Physics-informed machine learning for predictive turbulence modeling: using data to improve RANS modeled reynolds stresses, *Phys. Rev. Fluids* 2 (2016) 1–22.
- [54] J.L. Wu, H. Xiao, E. Paterson, Physics-informed machine learning approach for augmenting turbulence models: a comprehensive framework, *Phys. Rev. Fluids* 3 (2018) 074602.
- [55] J. Yan, W. Wang, P.X. Jiang, S. He, Direct numerical simulation of convective heat transfer in a vertical pipe for supercritical pressure CO<sub>2</sub>, in: Proceedings of the International Heat Transfer Conference, 16, 2018.
- [56] H.Y. Gu, M. Zhao, X. Cheng, Experimental studies on heat transfer to supercritical water in circular tubes at high heat fluxes, *Exp. Therm Fluid Sci.* 65 (2015) 22–32.
- [57] N. Launder, Three-dimensional and heat-loss effects on turbulent flow in a nominally two-dimensional cavity, *Int. J. Heat Fluid Flow* (1995).
- [58] H. Zhang, Z.R. Xie, Y.H. Yang, Numerical study on supercritical fluids flow and heat transfer under buoyancy, in: Proceedings of the International Topical Meeting on Nuclear Thermal-Hydraulics, Operation and Safety; NUTHOS-8, 2010.
- [59] M. Abadi, P. Barham, J. Chen, Z. Chen, X. Zhang, TensorFlow: A System for Large-Scale Machine Learning, USENIX Association, 2016.
- [60] V. Nair, G.E. Hinton, Rectified linear units improve restricted boltzmann machines vinod nair, in: Proceedings of the International Conference on Machine Learning, 2010.
- [61] Maas, A.L., Hannun, A.Y. and Ng, A.Y. 2013. Rectifier nonlinearities improve neural network acoustic models.
- [62] Z. Yang, T.H. Shih, New time scale based k-epsilon model for near-wall turbulence, *AIAA J.* (1993).
- [63] R.N. Xu, F. Luo, P.X. Jiang, Buoyancy effects on turbulent heat transfer of supercritical CO<sub>2</sub> in a vertical mini-tube based on continuous wall temperature measurements, *Int. J. Heat Mass Transf.* 110 (2017) 576–586.
- [64] Z.C. Wang, P.X. Jiang, R.N. Xu, Turbulent convection heat transfer analysis of supercritical pressure CO<sub>2</sub> flow in a vertical tube based on the field synergy principle, *Heat Transf. Eng.* 40 (2018) 476–486.
- [65] J. Fewster, Mixed Forced and free Convective Heat Transfer to Supercritical Pressure Fluids Flowing in Vertical Pipes, The University of Manchester, 1976.
- [66] E.N. Pis'menny, V.G. Razumovskiy, E.M. Maevskiy, A.E. Koloskov, I.L. Pioro, Heat transfer to supercritical water in gaseous state or affected by mixed convection in vertical tubes, in: Proceedings of the 14th International Conference on Nuclear Engineering, 2006.
- [67] W. Chang, X. Chu, A.F. Binte Shaik Fareed, S. Pandey, J. Luo, B. Weigand, E. Laijen, Heat transfer prediction of supercritical water with artificial neural networks, *Appl. Therm. Eng.* 131 (2018) 815–824.